Joint Beamforming Design for Secure RIS-Assisted IoT Networks

Hehao Niu, Zhi Lin, Zheng Chu, *Member, IEEE*, Zhengyu Zhu, *Senior Member, IEEE*, Pei Xiao, *Senior Member, IEEE*, Huan X. Nguyen, *Senior Member, IEEE*, Inkyu Lee, *Fellow, IEEE*, and Naofal Al-Dhahir, *Fellow, IEEE*

***Abstract*—This paper studies secure communication in an internet-of-things (IoT) network, where the confidential signal is sent by an active refracting reconfigurable intelligent surface (RIS)-based transmitter, and a passive reflective RIS is utilized to improve the secrecy performance of users in the presence of multiple eavesdroppers. Specifically, we aim to maximize the weighted sum secrecy rate by jointly designing the power allocation, transmit beamforming (BF) of the refracting RIS, and the phase shifts of the reflective RIS. To solve the non-convex optimization problem, we propose a linearization method to approximate the objective function into a linear form. Then, an alternating optimization (AO) scheme is proposed to jointly optimize the power allocation factors, BF vector and phase shifts, where the first one is found using the Lagrange dual method, while the latter two are obtained by utilizing the penalty dual decomposition method. Moreover, considering the demands of green and secure communications, by applying the Dinkelbach's method, we extend our proposed scheme to solving a secrecy energy maximization problem. Finally, simulation results demonstrate the effectiveness of the proposed design.**

***Index Terms*—RIS, secure communication, joint beamforming, alternating optimization, penalty dual decomposition**

This work was supported in part by the National Natural Science Foundation of China under Grant 61901490 and 62201592, in part by the Research Plan Project of NUDT under Grant ZK21-33, in part by the Young Elite Scientist Sponsorship Program of CAST under Grant 2021-JCJQ-QT-048, in part by the Macau Young Scholars Program under Grant AM2022011, in part by the National Research Foundation of Korea (NRF) grant funded by the Korea government (MSIT) (No. 2022R1A5A1027646), in part by the Project funded by China Postdoctoral Science Foundation under Grant 2020M682345, in part by the Henan Postdoctoral Foundation under Grant 202001015, in part by Sponsored by Program for Science & Technology Innovation Talents in Universities of Henan Province under Grant 23HASTIT019, in part by the Engineering and Physical Sciences Research Council (EPSRC) Project under Grant EP/P03456X/1, and in part by a British Council grant (ID# GGPVN 3.6) under the Going Global Partnerships programme. (*Corresponding author: Zhi Lin, Zheng Chu.*)

Hehao Niu is with the Sixty-third Research Institute, National University of Defense Technology, Nanjing 210007, China (e-mail: niuhaonupt@foxmail.com).

Zhi Lin is with the College of Electronic Engineering, National University of Defense Technology, Hefei 230037, China, and also with the School of Computer Science and Engineering, Macau University of Science and Technology, Macau 999078, China (e-mail: linzhi945@163.com).

Zheng Chu and Pei Xiao are with the Institute for Communication Systems, University of Surrey, Guildford GU2 7XH, U.K. (e-mail: andrew.chuzheng7@gmail.com; p.xiao@surrey.ac.uk).

Zhengyu Zhu is with the School of Electrical and Information Engineering, Zhengzhou University, Zhengzhou, 450001, China (e-mail: zhuzhengyu6@gmail.com).

Huan X. Nguyen is with the Faculty of Science and Technology, Middlesex University, London NW4 4BT, U.K. (e-mail: h.nguyen@mdx.ac.uk).

Inkyu Lee is with School of Electrical Engineering, Korea University, Seoul 02841, South Korea (e-mail: inkyu@korea.ac.kr).

Naofal Al-Dhahir is with the Department of Electrical and Computer Engineering, University of Texas at Dallas, Richardson, TX 75080 USA (email: aldhahir@utdallas.edu).

I. INTRODUCTION

Recent advances in wireless communications and smart sensing technologies have promoted the proliferation of the internet-of-things (IoT) to interconnect millions of physical objects to the Internet. Nowadays, IoT constitutes an integral part of the future Internet and has received much attention from both academia and industry [1].

Meanwhile, the reconfigurable intelligent surface (RIS) [2]-[4] has emerged as a promising technique for future wireless communications. Specifically, RIS is a planar array with massive low-cost reflective elements, which only consume ultra-low power in tuning the phase shifts and/or amplitudes of the incident signals to the RIS in a programmable manner, achieving smart reflection to the desired direction of the impinging electromagnetic (EM) waves [3]. Due to the reflective characteristic and simple hardware structure, the hardware cost and power consumption of RIS are much lower than the traditional transmitter or relay which include a radio frequency (RF) chain and power amplification components [4].

Recently, the work in [5] presented a joint active and passive beamforming (BF) design in a RIS-enhanced multiple-input single-output (MISO) network. In addition, [6] studied the multi-group multi-cast transmission in an RIS-assisted MISO system, where a fairness objective was tackled by a majorization-maximization (MM)-based method. Besides, for multiple-input multiple-output (MIMO) channels, spectral efficiency (SE) optimization in a RIS-MIMO network was studied in [7], where the authors proposed a manifold optimization-based method. Furthermore, the authors of [8] introduced energy efficiency (EE) optimization in RIS-assisted systems. Nowadays, RIS-assisted transmission has been investigated in various scenarios such as IoT networks [9], [10], simultaneous wireless information and power transfer (SWIPT) [11], non-orthogonal multiple access (NOMA) [12], hybrid terrestrial-aerial networks [13], [14], anti-jamming communications [15], [16], physical layer security communications [17], [18], and cognitive radio networks [19].

Furthermore, the authors of [20] focused on the outage constrained transmit power minimization problem in a RIS assisted MISO system, and proposed a stochastic gradient algorithm to solve it. Then, a two-timescale BF method was applied in [21] for RIS-assisted networks, where an active BF was designed with knowledge of instantaneous channel state information (CSI), and the phase shifts were obtained based on statistical CSI. Also, the RIS-aided MISO uplink network with imperfect CSI was studied in [22], where a penalty dual decomposition (PDD)-based design was developed to design the passive BF. From the EE perspective, the authors of [23] investigated optimization design in an uplink multiuser MIMO network with partial CSI by utilizing random matrix theory. Then, the tradeoff between EE and SE was studied in [24], where an iterative mean-square error minimization approach was adopted to find the RIS phase shifts.

Among the above works, RIS is commonly used to establish a cascaded link between the transmitter and receiver by reflecting the incident signal. On the other hand, RIS can also be applied in a transmitter design. The main advantage for the RIS-based transmitter architecture is that RF chains and antennas with power amplification are not required, leading to a significant reduction of the design complexity, hardware cost and power consumption. Generally speaking, modulation for RIS-based transmitters can be classified into two categories, namely, RIS-based direct modulation [25] and RIS-based space modulation [26]. For the former, RIS-enabled transmitters have successfully realized binary frequency shift keying (BFSK) modulation [27], quadrature phase shift keying (QPSK) modulation [28], and high order quadrature amplitude modulation (QAM) modulation [31]. While for the latter, [29] proposed MIMO transmission with RIS-enabled transmitter, and [30] proposed multi-channel transmission using space-time coding with RIS-enabled transmitter.

The above works are mainly based on the reflective RIS. Recently, some works have attempted to focus on the refracting RIS [32]-[34]. Particularly, according to [32], the reflective RIS would lead to occlusion for the feed source and it also has higher feed blockage compared to the refracting RIS, thus the latter is more suitable to deploy at the transmitter. Based on this observation, a refracting RIS-based transmitter structure was proposed for a multiuser downlink network in [33], where a joint power allocation and BF scheme maximized the information rate. Then in [34], a refracting RIS-based receiver structure was proposed for multiuser uplink network, where an alternating optimization (AO) algorithm was developed to maximize the system sum rate.

Security is an important aspect in wireless communications. RIS can enhance or weaken the reflecting signal power in different directions, thus is beneficial to achieve secure communication. Specifically, secrecy transmission was studied in [35] and [36] in RIS-aided MISO channels. Moreover, in [37] and [38], a robust secrecy design was presented in MISO networks, where a PDD-based method and concave-convex procedure (CCP)-based approach were proposed, respectively. Also, [39] proposed a MM-based algorithm to optimize the secure precoding and passive BF in RIS-aided MIMO channels. Then, in [40], the secrecy energy efficiency (SEE) optimization was developed in RIS-assisted networks, where the Dinkelbach's method based algorithms were proposed.

However, the transmitter in [35]-[40] based on traditional transmitter structures requires a large number of RF components and antennas. To compromise the secrecy performance and the system implementation complexity, we investigate secure communication of a double RIS-assisted network, where a refracting RIS is used at the transmitter to send the signal to the legitimate users, and a reflective RIS is used to reconfigure the channel environment. To be specific, we aim to maximize the weighted sum secrecy rate by jointly optimizing the transmit power allocation and BF, and the RIS phase shifts. To tackle this problem, a new linearization method is developed to transform the objective into a quadratic form. Then, we decouple the reformulated problem into several subproblems, where each subproblem can be solved efficiently. Finally, simulation results demonstrate that the sum secrecy rate of the proposed scheme is close to that of a traditional RF transmitter, while the former has simpler hardware architecture, lower power consumption and better SEE performance. We summarize our contributions as follows:

1) A novel multiuser downlink secrecy network is investigated, where a transmitter, which consists of a feed source and an active refracting RIS, sends confidential information to several legitimate IoT devices (IoTD), and a reflective RIS is adopted to strengthen the incident signal at the legitimate users in the presence of multiple eavesdroppers (Eves). This network architecture has the following benefits: 1) Compared to a traditional RF transmitter, the active refracting RIS is deployed to reduce power consumption; 2) The hardware cost of the refracting RIS is much lower than that of a traditional RF transmitter; 3) Reflective RIS is utilized to reconfigure the incident signal towards the intended direction and thus smartly enhance the degrees-of-freedom.
2) To measure the secure performance of the network, we formulate the weighted sum secrecy rate problem. To tackle the formulated problem, we adopt the first-order Taylor expansion to approximate the receiving rate of each IoTD and each Eve, thus we obtain an approximated objective with a quadratic form. Then, we decouple the reformulated problem into three subproblems. Specifically, for solving the power allocation optimization subproblem, the Lagrange dual method is adopted to obtain a semi-closed form solution by using the bisection search method for the dual variable. As for the second subproblem of optimizing the transmit BF of the refracting RIS, a two layer iterative algorithm using the PDD method and a computationally efficient element-wise Lagrange dual method are proposed to obtain the solutions, by considering both the cases of discrete and continuous coefficients. For the last subproblem, the passive BF of the reflecting RIS can be found by the PDD or element-wise Lagrange dual method. Building upon the above steps, a fast-converging alternating optimization (AO) method is developed, which converges in few iterations and is suitable for practical.
3) To meet the future green communication demands, we extend the proposed scheme to the SEE design. Specifically, by updating the slack variable in a one-dimensional search manner, we integrate the proposed algorithm with the Dinkelbach's method to solve the SEE maximization problem. Finally, our simulation results demonstrate the effectiveness of the proposed design and reveal several meaningful insights: 1) When given the same transmit

power budget without considering the power consumption of the static circuit, the traditional transmitter slightly outperforms the RIS-based transmitter in terms of SE, due to the spatial modulation ability provided by the RF chains and multiple antennas; 2) With the same system power consumption budget, our proposed scheme with RIS-based transmitter is superior to the traditional RF transmitter based scheme in terms of EE.

The remainder of this paper is organized as follows: Section II presents the signal model of a refracting RIS-enabled transmitter and the network model with a reflective RIS. The weighted sum secrecy rate maximization problem is formulated in Section III, where an AO scheme is proposed and the subproblems are solved using the corresponding algorithms. Then, Section IV extends the proposed design to the SEE design and Section V analyzes the computational complexity of the proposed AO scheme. Finally, Sections VI and VII present the simulation results and conclude the paper.

Notations: Throughout the paper, boldface lowercase and uppercase letters represent vectors and matrices, respectively. The transpose, conjugate, conjugate transpose, trace and the maximum eigenvalue of a matrix $\mathbf{A}$ are denoted as $\mathbf{A}^T$, $\mathbf{A}^*$, $\mathbf{A}^H$, $\mathrm{Tr}\left(\mathbf{A}\right)$, and $\lambda_{\max}\left(\mathbf{A}\right)$, respectively. $\|\cdot\|$ indicates the Euclidean norm and $\mathrm{Diag}\left(a_1,\ldots,a_N\right)$ equals a diagonal matrix with $a_1,\ldots,a_N$ being the main diagonal elements. $\mathbf{I}$ defines an identity matrix. $[x]^+$ means $\max\left\{0,x\right\}$. In addition, $\Re\left\{\cdot\right\}$, $|\cdot|$ and $\angle\left(\cdot\right)$ stand for the real part, the absolute value, and the angle of a complex variable, respectively. The letter j is used to represent $\sqrt{-1}$ when there is no ambiguity.

II. System Model and Problem Formulation

We start by introducing the system model for the considered multiuser MISO downlink network with multiple Eves. Then, we present the signal model for the refracting RIS-based transmitter in detail. Finally, a weighted sum secrecy rate optimization problem is formulated.

A. System Model for the Secrecy Multiuser Network

A downlink multiuser MISO system is illustrated in Fig. 1, which consists of a single refracting RIS-based transmitter, a reflective RIS, L legitimate IoTDs, and L Eves. The transmitter and the reflective RIS have M and N elements, respectively, while all the IoTDs and Eves are equipped with a single antenna. Besides, two RIS-controllers control the transmitter and the reflective RIS for CSI exchange and signal transmission. We denote $\mathbf{F}\in\mathbb{C}^{N\times M}$, $\mathbf{h}_{d,l}\in\mathbb{C}^{N\times 1}$, $\mathbf{g}_{d,l}\in\mathbb{C}^{N\times 1}$, $\mathbf{h}_{r,l}\in\mathbb{C}^{M\times 1}$, and $\mathbf{g}_{r,l}\in\mathbb{C}^{M\times 1}$ as the channels from the transmitter to the reflective RIS, from the transmitter to the l-th IoTD/Eve, the reflective RIS to the l-th IoTD/Eve $\left(l=1,\ldots,L\right)$, respectively. In addition, similar to [35] and [39], we assume that all CSI can be perfectly obtained by the transmitter in this paper.

The transmitter sends L independent data streams in the same frequency band simultaneously, where the confidential signal for the l-th IoTD is denoted as s_l, which is normalized as $\left|s_l\right|^2=1$. Here, artificial noise (AN) is transmitted to enhance the performance, defined by s_0 satisfying $\left|s_0\right|^2=1$.

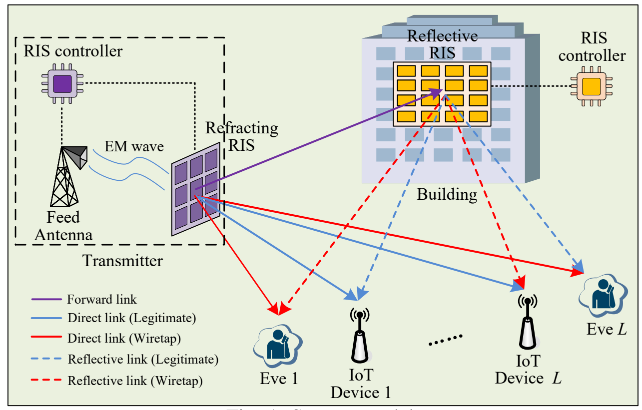

Fig. 1. System model.

Thus, the signal transmitted by the transmitter is given by $\mathbf{x}=\mathbf{w}\left(\sum_{l=1}^{L}a_l s_l+a_0 s_0\right)$, where a_l and a_0 represent the corresponding amplitude for s_l and s_0, and $\mathbf{w}$ is the BF coefficient of the refracting RIS, which will be discussed in the next subsection in detail.

The signals received by the l-th IoTD/Eve are, respectively, given by

$$\begin{aligned} y_{b,l}&=\left(\mathbf{h}_{d,l}^H+\mathbf{h}_{r,l}^H\mathbf{\Theta}^H\mathbf{F}\right)\mathbf{w}\sum_{i=0}^{L}a_i s_i+n_{b,l},\\ y_{e,l}&=\left(\mathbf{g}_{d,l}^H+\mathbf{g}_{r,l}^H\mathbf{\Theta}^H\mathbf{F}\right)\mathbf{w}\sum_{i=0}^{L}a_i s_i+n_{e,l}, \end{aligned}\tag{1}$$

where $n_{b,l}$ and $n_{e,l}$ are the zero-mean additive white Gaussian noise at the l-th IoTD/Eve, with power $\sigma_{b,l}^2$ and $\sigma_{e,l}^2$, respectively. Here, $\mathbf{\Theta}=\mathrm{diag}\left(\theta_1,\ldots,\theta_N\right)$ is the BF matrix for the reflective RIS, with $\theta_n=e^{j\varphi_n},\varphi_n\in\left[0,2\pi\right),\forall n\in\mathcal{N}\triangleq\left\{1,\ldots,N\right\}$, where φ_n represents the phase shift of the n-th element. Similar to [35], we assume that the amplitude of the reflective RIS is normalized due to its passive characteristic, and φ_n is equally spaced over $[0,2\pi)$, thus we have

$$\theta_n\in\mathcal{X}_d\triangleq\left\{\theta_n\left|\theta_n=e^{j\varphi_n},\varphi_n\in\mathcal{S}_\varphi\right.\right\},\tag{2}$$

where $\mathcal{S}_\varphi\triangleq\left\{0,\frac{2\pi}{2^{Q_\varphi}},\ldots,\frac{2\pi\left(2^{Q_\varphi}-1\right)}{2^{Q_\varphi}}\right\}$, and Q_φ denotes the number of quantization bits. In addition, when $Q_\varphi\to\infty$, the phase shift model in (2) converges to the continuous case, i.e., $\theta_n\in\mathcal{X}_c\triangleq\left\{\theta_n\left||\theta_n|=1\right.\right\}$ [42].

By denoting $\boldsymbol{\theta}=\left[\theta_1,\ldots,\theta_N\right]^T$, we obtain

$$\begin{aligned} \left(\mathbf{h}_{d,l}^H+\mathbf{h}_{r,l}^H\mathbf{\Theta}^H\mathbf{F}\right)\mathbf{w}&=\hat{\boldsymbol{\theta}}^H\mathbf{H}_l\mathbf{w},\\ \left(\mathbf{g}_{d,l}^H+\mathbf{g}_{r,l}^H\mathbf{\Theta}^H\mathbf{F}\right)\mathbf{w}&=\hat{\boldsymbol{\theta}}^H\mathbf{G}_l\mathbf{w}, \end{aligned}\tag{3}$$

where $\hat{\boldsymbol{\theta}}=\left[\boldsymbol{\theta}^H,1\right]^H$, $\mathbf{H}_l=\left[\mathrm{diag}\left(\mathbf{h}_{r,l}^H\right)\mathbf{F},\mathbf{h}_{d,l}^H\right]^T$, and $\mathbf{G}_l=\left[\mathrm{diag}\left(\mathbf{g}_{r,l}^H\right)\mathbf{F},\mathbf{g}_{d,l}^H\right]^T$, respectively.

Here, we assume that each Eve attempts to intercept the confidential signal sent to its nearest IoTD only, mainly due to the fact that the IoTD may spread in a region with a certain distance from each other. Thus, from Eve's point of view, it is more efficient for each Eve to intercept the signal send to the nearest IoTD rather than an IoTD located far away. Therefore, the secrecy rate for the l-th IoTD is given by

$$R_{s,l}=\left[\ln\left(1+\gamma_{b,l}\right)-\ln\left(1+\gamma_{e,l}\right)\right]^+,\tag{4}$$

and the signal-to-interference-plus-noise ratio (SINR) at the

l-th IoTD/Eve are, respectively, given by

$$\begin{aligned} \gamma_{b,l} &= \frac{\left|\hat{\boldsymbol{\theta}}^H \tilde{\mathbf{H}}_l \mathbf{w} a_l\right|^2}{\sum\limits_{i=0,i\neq l}^{L} \left|\hat{\boldsymbol{\theta}}^H \tilde{\mathbf{H}}_k \mathbf{w} a_i\right|^2 + 1}, \\ \gamma_{e,l} &= \frac{\left|\hat{\boldsymbol{\theta}}^H \tilde{\mathbf{G}}_l \mathbf{w} a_l\right|^2}{\sum\limits_{i=0,i\neq l}^{L} \left|\hat{\boldsymbol{\theta}}^H \tilde{\mathbf{G}}_k \mathbf{w} a_i\right|^2 + 1}, \end{aligned} \tag{5}$$

where $\tilde{\mathbf{H}}_l = \mathbf{H}_l/\sigma_{b,l}$ and $\tilde{\mathbf{G}}_l = \mathbf{G}_l/\sigma_{e,l}$.

In the rest of this work, we omit the operator $[\cdot]^+$ for simplicity, due to the non-negative nature of the optimal secrecy rate.

B. Signal Model for the Refracting RIS-based Transmitter

As shown in Fig. 1, the transmitter has a feed antenna which constantly emits EM waves (i.e., single-tone carrier signals), and a M element refracting RIS is used to adjust the amplitude and phase of the EM waves [33], [34]. We denote the refracting RIS BF vector as $\mathbf{w} = [w_1, \ldots w_M]^T \in \mathbb{C}^{M\times 1}$, where $w_m = \alpha_m e^{j\beta_m}$, with $\alpha_m \in [0,1], \beta_m \in [0, 2\pi), \forall m \in \mathcal{M} \triangleq \{1, \ldots, M\}$. Here, α_m and β_m denote the amplitude and phase response of the m-th element, respectively.

Discrete phase shifting is used in practical realizations due to its advantages in reducing hardware complexity, thus this paper assumes discrete values of α_m and β_m. Let Q_α and Q_β represent the number of quantization bits for α_m and β_m, respectively. Thus, we have

$$w_m \in \mathcal{W}_d \triangleq \left\{w_m \left| w_m = \alpha_m e^{j\beta_m}, \alpha_m \in \mathcal{S}_\alpha, \beta_m \in \mathcal{S}_\beta \right.\right\}, \tag{6}$$

where $\mathcal{S}_\alpha \triangleq \{\bar{\alpha}_1, \ldots, \bar{\alpha}_{Q_\alpha}\}$ denotes the amplitude set with $|\mathcal{S}_\alpha| = 2^{Q_\alpha}$, and $\mathcal{S}_\beta \triangleq \left\{0, \frac{2\pi}{2^{Q_\beta}}, \ldots, \frac{2\pi\left(2^{Q_\beta}-1\right)}{2^{Q_\beta}}\right\}$ denotes the phase set, i.e., the discrete phase shifts are equally valued over $[0, 2\pi)$ [43]. Note that $\mathcal{S}_\alpha = \{1\}$ when $Q_\alpha = 0$, while $\mathcal{S}_\alpha = \{0, 1\}$ represents an on/off operation when $Q_\alpha = 1$ [43]. Moreover, when $Q_\alpha \to \infty$ and $Q_\beta \to \infty$, the model in (6) turns into a continuous coefficients case, i.e., $w_m \in \mathcal{W}_c \triangleq \{w_m \,||w_m| \leq 1\}$ [33], which can be treated as an upper bound on the performance.

C. Problem Formulation

Our objective is to maximize the weighted sum secrecy rate by jointly designing the power allocation $\{a_l\}_{l=0}^L$, the BF vector $\mathbf{w}$, and the RIS phase shift $\hat{\boldsymbol{\theta}}$, which is written as

$$\max_{\{a_l\}_{l=0}^L, \mathbf{w}, \hat{\boldsymbol{\theta}}} R_s \triangleq \sum_{l=1}^{L} \varrho_l \left(\ln(1+\gamma_{b,l}) - \ln(1+\gamma_{e,l})\right) \tag{7a}$$

$$\text{s.t.} \ \sum_{l=0}^{L} a_l^2 \leq P_s, a_l \geq 0, \forall l, \tag{7b}$$

$$w_m \in \mathcal{W}_d, \forall m \in \mathcal{M}, \tag{7c}$$

$$\theta_n \in \mathcal{X}_d, \forall n \in \mathcal{N}, \hat{\theta}_{N+1} = 1, \tag{7d}$$

where ϱ_l is the weight for the l-th IoTD satisfies $\left(0 \leq \varrho_l \leq 1, \sum_{l=1}^{L} \varrho_l = 1\right)$, and P_s indicates the transmit power budget for the transmitter.

III. The Proposed Design

Due to the non-concave form (7a), the optimization problem (7) is hard to solve. In the following, the objective function (7a) is firstly linearized and problem (7) is decomposed to three subproblems. Then, we propose an iterative algorithm to update the variables until convergence.

A. Lower Bound on the Objective

We aim to find a lower bound on (7a) around the given point $\left\{\{a_l^t\}_{l=0}^L, \mathbf{w}^t, \hat{\boldsymbol{\theta}}^t\right\}$ at the t-th iteration. The following two Lemmas can be used to transform $R_{s,l}$ into a solvable formulation.

Lemma 1 [44]: For any u and v, we have

$$\begin{aligned} \ln\left(1 + \frac{|u|^2}{v}\right) &\geq \ln\left(1 + \frac{|\bar{u}|^2}{\bar{v}}\right) - \frac{|\bar{u}|^2}{\bar{u}} \\ &+ \frac{2\Re\{\bar{u}^* u\}}{\bar{v}} - \frac{|\bar{u}|^2 \left(v + |u|^2\right)}{\bar{v}\left(\bar{v} + |\bar{u}|^2\right)}, \end{aligned} \tag{8}$$

where $\{\bar{u}, \bar{v}\}$ are fixed points.

Based on Lemma 1, a lower bound on the receiving rate of the l-th IoTD is expressed as

$$\begin{aligned} \ln(1+\gamma_{b,l}) &\geq \ln\left(1 + \frac{|x_l^t|^2}{y_l^t}\right) - \frac{|x_l^t|^2}{y_l^t} \\ &+ 2\frac{\Re\left\{(x_l^t)^* x_l\right\}}{y_l^t} - \frac{|x_l^t|^2 \left(y_l + |x_l|^2\right)}{y_l^t\left(y_l^t + |x_l^t|^2\right)}, \end{aligned} \tag{9}$$

where $x_l = \hat{\boldsymbol{\theta}}^H \tilde{\mathbf{H}}_l \mathbf{w} a_l$, $y_l = \sum_{i=0,i\neq l}^{L} \left|\hat{\boldsymbol{\theta}}^H \tilde{\mathbf{H}}_l \mathbf{w} a_i\right|^2 + 1$, $x_l^t = \left(\hat{\boldsymbol{\theta}}^t\right)^H \tilde{\mathbf{H}}_l \mathbf{w}^t a_l^t$, and $y_l^t = \sum_{i=0,i\neq l}^{L} \left|\left(\hat{\boldsymbol{\theta}}^t\right)^H \tilde{\mathbf{H}}_l \mathbf{w}^t a_i^t\right|^2 + 1$, respectively. Then, we obtain

$$-\ln(1+\gamma_{e,l}) = \ln\left(1 + \sum_{i=0,i\neq k}^{L} \left|\hat{\boldsymbol{\theta}}^H \tilde{\mathbf{G}}_l \mathbf{w} a_i\right|^2\right) - \ln(1+z_l), \tag{10}$$

where $z_l = \sum_{i=0}^{L} \left|\hat{\boldsymbol{\theta}}^H \tilde{\mathbf{G}}_l \mathbf{w} a_i\right|^2$. To handle (10), the following Lemma is introduced.

Lemma 2: For any $\{u_i\}_{i=1}^L$, we have

$$\begin{aligned} \ln\left(1 + \sum_{i=1}^{L} |u_i|^2\right) &\geq \ln\left(1 + \sum_{i=1}^{L} |\bar{u}_i|^2\right) - \sum_{i=1}^{L} |\bar{u}_i|^2 \\ &+ \sum_{i=1}^{L} 2\Re\left\{\bar{u}_i^* u_i\right\} - \frac{\sum\limits_{i=1}^{L} |\bar{u}_i|^2 \left(1 + \sum\limits_{i=1}^{L} |u_i|^2\right)}{1 + \sum\limits_{i=1}^{L} |\bar{u}_i|^2}, \end{aligned} \tag{11}$$

where $\{\bar{u}_i\}_{i=1}^L$ is a fixed point.

The proof of Lemma 2 is straightforward. In fact, by using Lemma 1 with $v = \bar{v} = 1$, we have

$$\begin{aligned} \ln\left(1 + |u|^2\right) &\geq \ln\left(1 + |\bar{u}|^2\right) - |\bar{u}|^2 \\ &+ 2\Re\{\bar{u}^* u\} - \frac{|\bar{u}|^2 \left(1 + |u|^2\right)}{\left(1 + |\bar{u}|^2\right)}. \end{aligned} \tag{12}$$

Then, by fixing u_i for $i = 2, \ldots, L$, it follows that

$$\ln\left(S + |u_1|^2\right) \geq \ln\left(S + |\bar{u}_1|^2\right) - |\bar{u}_1|^2 + 2\Re\{\bar{u}_1^* u_1\} - \frac{|\bar{u}_1|^2\left(S + |u_1|^2\right)}{\left(S + |\bar{u}_1|^2\right)}, \tag{13}$$

where $S = 1 + \sum_{i=2}^{L} |u_i|^2$. Thus, by using (13) for u_i with fixed other u_i from $i = 2$ to $i = L$, we obtain (11).

According to (11), we obtain the following inequality

$$\begin{aligned}
&\ln\left(1 + \sum_{i=0, i\neq l}^{L} \left|\hat{\boldsymbol{\theta}}^H \tilde{\mathbf{G}}_l \mathbf{w} a_i\right|^2\right) \\
&\geq \ln\left(1 + \sum_{i=0, i\neq l}^{L} \left|\left(\hat{\boldsymbol{\theta}}^t\right)^H \tilde{\mathbf{G}}_l \mathbf{w}^t a_i^t\right|^2\right) \\
&- \sum_{i=0, i\neq l}^{L} \left|\left(\hat{\boldsymbol{\theta}}^t\right)^H \tilde{\mathbf{G}}_l \mathbf{w}^t a_i^t\right|^2 \\
&+ \sum_{i=0, i\neq l}^{L} 2\Re\left\{a_i \mathbf{w}^H \tilde{\mathbf{G}}_l^H \hat{\boldsymbol{\theta}} \left(\hat{\boldsymbol{\theta}}^t\right)^H \tilde{\mathbf{G}}_l \mathbf{w}^t a_i^t\right\} \\
&- \frac{c_l^t}{1 + c_l^t}\left(1 + \sum_{i=0, i\neq l}^{L} \left|\hat{\boldsymbol{\theta}}^H \tilde{\mathbf{G}}_l \mathbf{w} a_i\right|^2\right),
\end{aligned} \tag{14}$$

where $c_l^t = \sum_{i=0, i\neq l}^{L} \left|\left(\hat{\boldsymbol{\theta}}^t\right)^H \tilde{\mathbf{G}}_l \mathbf{w}^t a_i^t\right|^2$.

Next, we focus on the second term in (10). Due to the concavity of the logarithm function $\ln(u) \leq \ln(u_0) + \frac{u}{u_0} - 1$, we have [45], [46]

$$-\ln(1 + z_l) \geq -\ln\left(1 + z_l^t\right) - \frac{1 + z_l}{1 + z_l^t} + 1, \tag{15}$$

where $z_l^t = \sum_{i=0}^{L} \left|\left(\hat{\boldsymbol{\theta}}^t\right)^H \tilde{\mathbf{G}}_l \mathbf{w}^t a_i^t\right|^2$.

Thus, we obtain the following problem

$$\begin{aligned}
\min_{\{a_l\}_{l=0}^L, \mathbf{w}, \hat{\boldsymbol{\theta}}} \sum_{l=1}^{L} \varrho_l \Bigg\{ & \frac{c_l^t}{1 + c_l^t}\left(\sum_{i=0, i\neq l}^{L} \left|\hat{\boldsymbol{\theta}}^H \tilde{\mathbf{G}}_l \mathbf{w} a_i\right|^2\right) \\
& + \frac{|x_l^t|^2 \sum_{i=0}^{L} \left|\hat{\boldsymbol{\theta}}^H \tilde{\mathbf{H}}_l \mathbf{w} a_i\right|^2}{y_l^t\left(y_l^t + |x_l^t|^2\right)} + \frac{\sum_{i=0}^{L} \left|\hat{\boldsymbol{\theta}}^H \tilde{\mathbf{G}}_l \mathbf{w} a_i\right|^2}{1 + z_l^t} \\
& - \sum_{i=0, i\neq l}^{L} 2\Re\left\{a_i \mathbf{w}^H \tilde{\mathbf{G}}_l^H \hat{\boldsymbol{\theta}} \left(\hat{\boldsymbol{\theta}}^t\right)^H \tilde{\mathbf{G}}_l \mathbf{w}^t a_i^t\right\} \\
& - \frac{2\Re\left\{a_l \mathbf{w}^H \tilde{\mathbf{H}}_l^H \hat{\boldsymbol{\theta}} \left(\hat{\boldsymbol{\theta}}^t\right)^H \tilde{\mathbf{H}}_l \mathbf{w}^t a_l^t\right\}}{y_l^t} \Bigg\}
\end{aligned} \tag{16a}$$

$$\text{s.t.} \quad (7\text{b}) - (7\text{d}). \tag{16b}$$

Therefore, the original problem (7) has been converted to an approximated problem (16). In the following, we will further decouple (16) into several subproblems and propose an AO scheme to solve (16).

B. Power Allocation Optimization

Now, the power allocation subproblem is considered. To be specific, around the given point $\left\{\{a_l^t\}_{l=0}^L, \mathbf{w}^t, \hat{\boldsymbol{\theta}}^t\right\}$, the power allocation problem can be formulated as

$$\begin{aligned}
\min_{\{a_l\}_{l=0}^L} \quad & \sum_{l=0}^{L} a_l^2 T_l - 2 a_l t_l \\
\text{s.t.} \quad & (7\text{b}),
\end{aligned} \tag{17}$$

where $\{T_l, t_l\}_{l=0}^L$ are obtained by merging related items with respect to $\{a_l\}_{l=0}^L$, which is given by

$$\begin{aligned}
T_0 &= \sum_{i=1}^{L} \frac{\varrho_i |x_i^t|^2 \left|\left(\hat{\boldsymbol{\theta}}^t\right)^H \tilde{\mathbf{H}}_i \mathbf{w}^t\right|^2}{y_i^t\left(y_i^t + |x_i^t|^2\right)} + \\
&\sum_{i=1}^{L} \frac{\varrho_i \left|\left(\hat{\boldsymbol{\theta}}^t\right)^H \tilde{\mathbf{G}}_i \mathbf{w}^t\right|^2}{1 + z_i^t} + \sum_{i=1}^{L} \frac{\varrho_i c_i^t \left|\left(\hat{\boldsymbol{\theta}}^t\right)^H \tilde{\mathbf{G}}_i \mathbf{w}^t\right|^2}{1 + c_i^t}, \\
t_0 &= \sum_{i=1}^{L} \varrho_i \Re\left\{\left(\mathbf{w}^t\right)^H \tilde{\mathbf{G}}_i^H \boldsymbol{\theta}^t \left(\hat{\boldsymbol{\theta}}^t\right)^H \tilde{\mathbf{G}}_i \mathbf{w}^t a_0^t\right\}, \\
T_l &= T_0 - \frac{\varrho_l c_l^t \left|\left(\hat{\boldsymbol{\theta}}^t\right)^H \tilde{\mathbf{G}}_l \mathbf{w}^t\right|^2}{1 + c_l^t}, \forall l, \\
t_l &= \sum_{i=1, i\neq l}^{L} \varrho_i \Re\left\{\left(\mathbf{w}^t\right)^H \tilde{\mathbf{G}}_i^H \boldsymbol{\theta}^t \left(\hat{\boldsymbol{\theta}}^t\right)^H \tilde{\mathbf{G}}_i \mathbf{w}^t a_l^t\right\} \\
&+ \frac{\varrho_l \Re\left\{\left(\mathbf{w}^t\right)^H \tilde{\mathbf{H}}_l^H \boldsymbol{\theta}^t \left(\hat{\boldsymbol{\theta}}^t\right)^H \tilde{\mathbf{H}}_l \mathbf{w}^t a_l^t\right\}}{y_l^t}, \forall l.
\end{aligned} \tag{18}$$

Although problem (17) is convex and can be solved by the optimization toolbox CVX [48], it is not computationally efficient. Here, we propose a more efficient method by using the Lagrange dual approach. Firstly, we derive the Lagrange function of (17) as

$$\mathcal{L}\left(\{a_l\}_{l=0}^L, \lambda\right) = \sum_{l=0}^{L} \left(a_l^2 T_l - 2 a_l t_l\right) + \lambda\left(\sum_{l=0}^{L} a_l^2 - P_s\right), \tag{19}$$

where $\lambda \geq 0$ is the dual variable with respect to (16b). Hence, we define the following dual function

$$g(\lambda) = \min_{\{a_l\}_{l=0}^L} \mathcal{L}\left(\{a_l\}_{l=0}^L, \lambda\right), \tag{20}$$

and the dual problem is formulated as $\max_{\lambda} g(\lambda)$ s.t. $\lambda \geq 0$. For a given λ, we define the corresponding solution to (20) as $\{a_l(\lambda)\}_{l=0}^L$. Then, by computing the first-order derivative with respect to a_l, we obtain the following equation

$$a_l(\lambda) = \frac{-t_l}{\lambda + T_l}, \forall l. \tag{21}$$

In addition, the optimal $\lambda^\star$ needs to satisfy the complementary slackness condition $\lambda^\star\left(\sum_{l=0}^{L} a_l^2(\lambda^\star) - P_s\right) = 0$, which can be solved by considering the following two cases

1) If $\sum_{l=0}^{L} a_l^2(0) \leq P_s$ holds true, then the optimal $\lambda^\star$ is 0.
2) Otherwise, $\lambda^\star$ can be obtained by solving the equation $\sum_{l=0}^{L} a_l^2(\lambda) = P_s$, e.g., $\sum_{l=0}^{L} t_l^2 \Big/ (\lambda + T_l)^2 = P_s$. It does not appear possible to derive a closed-form solution. However, by calculating the first-order derivative, it can be easily proved that $\sum_{l=0}^{L} t_l^2 \Big/ (\lambda + T_l)^2$ decreases monotonically with respect to λ when $\lambda \geq 0$. Thus, the bisection search method is applied to select λ. In addition,

an upper bound on λ can be found by setting $T_l = 0, \forall l$. Then, according to $\sum_{l=0}^{L} t_l^2 \big/ \lambda^2 = P_s$, an upper bound on λ is $\lambda^{ub} = \sqrt{\sum_{l=0}^{L} t_l^2 \big/ P_s}$.

The detailed steps for finding $\{a_l\}_{l=0}^{L}$ and λ are summarized in Algorithm 1.

Algorithm 1 The Lagrange Dual Algorithm.

1: Initialize $\lambda^{lb} = 0$ and $\lambda^{ub} = \sqrt{\sum_{l=0}^{L} t_l^2 \big/ P_s}$;
2: Calculate $\{a_l(0)\}_{l=0}^{L}$ according to (21). **If** $P(0) \le P_s$, $\lambda^\star = 0$. **Otherwise**, move to step 3;
3: **repeat**
4: Calculate $\lambda = \left(\lambda^{lb} + \lambda^{ub}\right)/2$;
5: Obtain $\{a_l(0)\}_{l=0}^{L}$ according to (21);
6: Calculate $P(\lambda)$ and set $\begin{cases} \lambda^{lb} = \lambda, \text{ if } P(\lambda) \ge P_s, \\ \lambda^{ub} = \lambda, \text{ else.} \end{cases}$
7: **until If** $\left|\lambda^{lb} - \lambda^{ub}\right|$ is below a certain threshold ε, **terminate**, **otherwise**, move to Step 4.
8: **Output** $\left\{\lambda^\star, \{a_l^\star\}_{l=0}^{L}\right\}$.

C. Transmit BF Optimization

Here, we focus on the optimization of the transmit BF $\mathbf{w}$. With fixed $\left\{\{a_l^t\}_{l=0}^{L}, \mathbf{w}^t, \hat{\boldsymbol{\theta}}^t\right\}$, we formulate the following problem

$$\begin{aligned} \min_{\mathbf{w}} \ & \mathbf{w}^H \mathbf{A} \mathbf{w} - 2\Re\left\{\mathbf{w}^H \mathbf{b}\right\} \\ \text{s.t.} \ & (7c), \end{aligned} \tag{22}$$

where $\mathbf{A} = \sum_{l=1}^{L} \varrho_l \mathbf{A}_l$ and $\mathbf{b} = \sum_{l=1}^{L} \varrho_l \mathbf{b}_l$. Here, $\mathbf{A}_l$ and $\mathbf{B}_l$ are, respectively, given by

$$\begin{aligned} \mathbf{A}_l = & \frac{|x_l^t|^2 \sum\limits_{i=0}^{L} (a_i^t)^2 \tilde{\mathbf{H}}_l^H \hat{\boldsymbol{\theta}}^t \left(\hat{\boldsymbol{\theta}}^t\right)^H \tilde{\mathbf{H}}_l}{y_l^t \left(y_l^t + |x_l^t|^2\right)} \\ & + \frac{\sum\limits_{i=0}^{L} (a_i^t)^2 \tilde{\mathbf{G}}_l^H \hat{\boldsymbol{\theta}}^t \left(\hat{\boldsymbol{\theta}}^t\right)^H \tilde{\mathbf{G}}_l}{1 + z_l^t} \\ & + \frac{c_l^t \sum\limits_{i=0, i\neq l}^{L} (a_i^t)^2 \tilde{\mathbf{G}}_l^H \hat{\boldsymbol{\theta}}^t \left(\hat{\boldsymbol{\theta}}^t\right)^H \tilde{\mathbf{G}}_l}{1 + c_l^t}, \forall l, \\ \mathbf{b}_l = & \frac{\tilde{\mathbf{H}}_l^H \hat{\boldsymbol{\theta}}^t \left(\hat{\boldsymbol{\theta}}^t\right)^H \tilde{\mathbf{H}}_l \mathbf{w}^t (a_l^t)^2}{y_l^t} \\ & + \sum_{i=0, i\neq l}^{L} \tilde{\mathbf{G}}_l^H \hat{\boldsymbol{\theta}}^t \left(\hat{\boldsymbol{\theta}}^t\right)^H \tilde{\mathbf{G}}_l \mathbf{w}^t (a_i^t)^2, \forall l. \end{aligned} \tag{23}$$

In fact, the semidefinite relaxation (SDR) method [40] has been adopted to handle problems similar to (22). Here, we propose a PDD-based scheme to optimize these variables, which can find a closed-form solution with relatively lower computational complexity. To be specific, the slack variable $\mathbf{r} = [r_1, \ldots, r_M]^T \in \mathbb{C}^{M\times 1}$ is introduced to (22), where $r_m = \alpha_m e^{j\beta_m}, \forall m \in \mathcal{M}$ satisfies $\mathbf{r} = \mathbf{w}$. Then, we reformulate (22) as

$$\begin{aligned} \min_{\mathbf{w},\mathbf{r}} \ & \mathbf{w}^H \mathbf{A} \mathbf{w} - 2\Re\left\{\mathbf{w}^H \mathbf{b}\right\} \\ \text{s.t.} \ & \mathbf{w} = \mathbf{r}, r_m \in \mathcal{W}_d, \forall m \in \mathcal{M}. \end{aligned} \tag{24}$$

The augmented Lagrange (AL) problem of (24) is given by

$$\begin{aligned} \min_{\mathbf{w},\mathbf{r}} \ & \mathbf{w}^H \mathbf{A} \mathbf{w} - 2\Re\left\{\mathbf{w}^H \mathbf{b}\right\} + \frac{1}{2\rho}\|\mathbf{w} - \mathbf{r} + \rho\boldsymbol{\lambda}\|^2 \\ \text{s.t.} \ & \|\mathbf{w}\|^2 \le M, r_m \in \mathcal{W}_d, \forall m \in \mathcal{M}, \end{aligned} \tag{25}$$

where $\rho \ge 0$ and $\boldsymbol{\lambda} \in \mathbb{C}^{M\times 1}$ are the penalty factor and the scaled dual variable associated with the constraint $\mathbf{w} = \mathbf{r}$, respectively. In fact, it has been proved that when $\rho \le 0.5/\lambda_{\max}(\mathbf{A})$, (25) is bounded and can be guaranteed to converge [47]. However, when the value of $\lambda_{\max}(\mathbf{A})$ is large, the initial penalty term $0.5/\rho$ needs to be large enough, thus restricting the search space of (25). As an alternative, a new constraint $\|\mathbf{w}\|^2 \le M$ is introduced to expand the search space without loss of the optimality since $|w_m| \le 1$ [21].

The PDD procedure is composed of two layers. In the outer layer, we update ρ and $\boldsymbol{\lambda}$, while in the inner layer, we decouple (25) into two blocks and optimize $\mathbf{w}$ and $\mathbf{r}$ alternately. Specifically, in the inner layer, we first optimize $\mathbf{w}$ with given $\mathbf{r}$. The optimization problem is written as

$$\begin{aligned} \min_{\mathbf{w}} \ & \mathbf{w}^H \mathbf{A} \mathbf{w} - 2\Re\left\{\mathbf{w}^H \mathbf{b}\right\} + \frac{1}{2\rho}\|\mathbf{w} - \mathbf{r} + \rho\boldsymbol{\lambda}\|^2 \\ \text{s.t.} \ & \|\mathbf{w}\|^2 \le M. \end{aligned} \tag{26}$$

(26) is convex and the optimal $\mathbf{w}$ is obtained by:

$$\mathbf{w} = \begin{cases} \mathbf{d}, \text{ if } \|\mathbf{d}\|^2 \le M, \\ \sqrt{M}\mathbf{d} \big/ \|\mathbf{d}\|, \text{ else,} \end{cases} \tag{27}$$

where $\mathbf{d} = \left(2\mathbf{A} + \frac{\mathbf{I}}{\rho}\right)^{-1}\left(2\mathbf{b} + \frac{\mathbf{r}}{\rho} - \lambda\right)$.

Then, we focus on the optimization of $\mathbf{r}$ with given $\mathbf{w}$. By ignoring constant terms, the problem is given by

$$\min_{\mathbf{r}} \ \|\mathbf{w} - \mathbf{r} + \rho\boldsymbol{\lambda}\|^2 \tag{28a}$$

$$\text{s.t.} \ r_m \in \mathcal{W}_d, \forall m \in \mathcal{M}. \tag{28b}$$

Since the inner components of $\mathbf{r}$ are decoupled in (28a) and (28b), the optimal solution of (28) is $r_m^\star = \bar{\alpha}_m e^{j\angle\bar{\beta}_m}$, where $\bar{\beta}_m = \arg\min\limits_{\beta_m \in \mathcal{S}_\beta} |\beta_m - \angle(w_m + \rho\lambda_m)|$ and $\bar{\alpha}_m = \arg\min\limits_{\angle\alpha_m \in \mathcal{S}_\alpha} \left|\alpha_m e^{j\angle\bar{\beta}_m} - w_m - \rho\lambda_m\right|$ [43].

Hence, $\mathbf{w}$ and $\mathbf{r}$ can be iteratively computed until convergence, which completes the inner layer optimization. For the outer layer iteration, $\boldsymbol{\lambda}$ and ρ are updated using

$$\boldsymbol{\lambda} \leftarrow \boldsymbol{\lambda} + (\mathbf{w} - \mathbf{r})/\rho, \text{ and } \rho \leftarrow \tau\rho, \tag{29}$$

respectively, where $\tau < 1$ is a constant scaling factor that is used to control the value of the penalty term in each outer iteration [21]. The PDD scheme is summarized in Algorithm 2, and the convergence has been proved in [49].

Next, we tackle the BF optimization in the continuous coefficient case. Specifically, the problem is given by

$$\min_{\mathbf{w}} \ \mathbf{w}^H \mathbf{A} \mathbf{w} - 2\Re\left\{\mathbf{w}^H \mathbf{b}\right\} \tag{30a}$$

$$\text{s.t.} \ |w_m| \le 1, \forall m \in \mathcal{M}. \tag{30b}$$

Then, the PDD scheme can be used to transform (30) as

$$\begin{aligned} \min_{\mathbf{r}} \ & \|\mathbf{w} - \mathbf{r} + \rho\boldsymbol{\lambda}\|^2 \\ \text{s.t.} \ & |r_m| \le 1, \forall m \in \mathcal{M}. \end{aligned} \tag{31}$$

(31) is a projection problem and the optimal solution is

$$r_m = \begin{cases} d_m, \text{ if } |d_m| \le 1, \\ d_m/|d_m|, \text{ else,} \end{cases} \tag{32}$$

where $d_m = w_m + \rho\lambda_m$.

Here, we resort to a more efficient approach to design w_m. Specifically, we adopt the Lagrange dual optimization to w_m

This article has been accepted for publication in IEEE Internet of Things Journal. This is the author's version which has not been fully edited and content may change prior to final publication. Citation information: DOI 10.1109/JIOT.2022.3210115

Algorithm 2 The PDD Algorithm.

1: Initialize $\left\{\mathbf{w}^0, \mathbf{r}^0, \boldsymbol{\lambda}^0, \rho^0\right\}$ and set $i=1$;
2: **repeat**
3: Set $\mathbf{w}^{i-1,\ell}=\mathbf{w}^{i-1}$, $\mathbf{r}^{i-1,\ell}=\mathbf{r}^{i-1}$, and $\ell=0$;
4: **repeat**
5: Update $\mathbf{w}^{i-1,\ell+1}$ by (27);
6: Update $\mathbf{r}^{i-1,\ell+1}$ by (32);
7: **until** Convergence.
8: $\mathbf{w}^i \leftarrow \mathbf{w}^{i-1,\ell}$, $\mathbf{r}^i \leftarrow \mathbf{r}^{i-1,\ell}$;
9: $\boldsymbol{\lambda}^i \leftarrow \boldsymbol{\lambda}^{i-1}+\left(\mathbf{w}^i-\mathbf{r}^i\right)/\rho^i$, $\rho^i \leftarrow \tau\rho^{i-1}$;
10: $i \leftarrow i+1$;
11: **until** $\left\|\mathbf{w}^\ell-\mathbf{r}^\ell\right\| \leq \varepsilon$ or exceed the maximum number of iteration.
12: **Output** $\{\mathbf{w}^\star, \mathbf{r}^\star\}$.

by fixing the coefficients for other $w_l, \forall l \neq m$, which has a semi-closed-form solution. Particularly, $\mathbf{w}^H\mathbf{A}\mathbf{w}$ and $\mathbf{w}^H\mathbf{b}$ can be reformulated as

$$\begin{aligned}\mathbf{w}^H\mathbf{A}\mathbf{w} &= \sum_{i=1}^{M}\sum_{j=1}^{M} w_i^* a_{i,j} w_j = w_m^* a_{m,m} w_m \\ &+ 2\Re\left\{\sum_{j=1,j\neq m}^{M} w_m^* a_{m,j} w_j\right\} + \sum_{\substack{i=1,\\ i\neq m}}^{M}\sum_{\substack{j=1,\\ j\neq m}}^{M} w_i^* a_{i,j} w_j,\end{aligned} \tag{33a}$$

$$\mathbf{w}^H\mathbf{b} = \sum_{i=1}^{M} w_i^* b_i = w_m^* b_m + \sum_{i=1,i\neq m}^{M} w_i^* b_i, \tag{33b}$$

where $a_{i,j}$ denotes the (i,j)-th element of $\mathbf{A}$ and b_i represents the i-th entry of $\mathbf{b}$, respectively.

Then, by substituting (33a) and (33b) into (30a) and ignoring the irrelevant terms, we arrive at the following optimization problem with respect to w_m, where $w_i\ (i \neq m)$ is fixed

$$\min_{w_m} \quad w_m^* a_{m,m} w_m - 2\Re\left\{w_m^* \tilde{b}_m\right\} \tag{34a}$$

$$\text{s.t.} \quad |w_m| \leq 1, \forall m \in \mathcal{M}, \tag{34b}$$

where $\tilde{b}_m = b_m - \sum_{j=1,j\neq m}^{M} a_{m,j} w_j$. The Lagrange function of (34) is given as

$$\mathcal{L}(w_m,\lambda) = w_m^* a_{m,m} w_m - 2\Re\left\{w_m^* \tilde{b}_m\right\} + \lambda\left(w_m^* w_m - 1\right), \tag{35}$$

where λ is a dual variable.

Then, based on $|w_m|$, we have three cases:

1) $0 < |w_m| < 1$: we have $\lambda = 0$ according to the complementary slackness optimization. Then, by calculating the first-order derivative, we obtain $w_m^\star = \tilde{b}_m \big/ a_{m,m}$. It should be noted that if $\left|\tilde{b}_m \big/ a_{m,m}\right| \geq 1$, both w_m and the value of objective function are actually infeasible.
2) $|w_m| = 1$: since (34a) can be simplified as $a_{m,m} - 2\Re\left\{w_m^* \tilde{b}_m\right\}$, the optimal solution is $w_m^\star = \tilde{b}_m \big/ \left|\tilde{b}_m\right|$.
3) $|w_m| = 0$: we have $w_m^\star = 0$.

By comparing the objective values in these cases, we obtain the optimal solution to (34). Then, we successively optimize each w_m using the Lagrange dual method until convergence.

The above element-wise Lagrange dual method is summarized in Algorithm 3.

Algorithm 3 The element-wise Lagrange dual method.

1: Initialize $\mathbf{w}^0$, and set $q=0$;
2: **repeat**
3: **for** $m=1$ **to** M;
4: Computer $\tilde{b}_m$ and the corresponding objective for cases 1-3; Select the optimal w_m;
5: **end**
6: $q \leftarrow q+1$;
7: **until** $\left\|\mathbf{w}^q-\mathbf{w}^{q-1}\right\| \leq \varepsilon$ or exceed the maximum number of iterations.
8: **Output** $\mathbf{w}^\star$.

D. Reflecting BF optimization

To optimize $\hat{\boldsymbol{\theta}}$ around a given point $\left\{\left\{a_l^t\right\}_{l=0}^{L}, \mathbf{w}^t, \hat{\boldsymbol{\theta}}^t\right\}$, we have the following problem:

$$\begin{aligned}\min_{\hat{\boldsymbol{\theta}}} \ & \hat{\boldsymbol{\theta}}^H \boldsymbol{\Omega} \hat{\boldsymbol{\theta}} - 2\Re\left\{\hat{\boldsymbol{\theta}}^H \boldsymbol{\phi}\right\} \\ \text{s.t.} \ & \text{(7d)},\end{aligned} \tag{36}$$

where $\boldsymbol{\Omega} = \sum_{l=1}^{L} \varrho_l \boldsymbol{\Omega}_l$ and $\boldsymbol{\phi} = \sum_{l=1}^{L} \varrho_l \boldsymbol{\phi}_l$, with $\boldsymbol{\Omega}_l$ and $\boldsymbol{\phi}_l$ are given by

$$\begin{aligned}\boldsymbol{\Omega}_l = & \frac{\left|x_l^t\right|^2 \sum_{i=0}^{L} \left(a_i^t\right)^2 \tilde{\mathbf{H}}_l \mathbf{w}^t \left(\mathbf{w}^t\right)^H \tilde{\mathbf{H}}_l^H}{y_l^t\left(y_l^t + \left|x_l^t\right|^2\right)} \\ & + \frac{\sum_{i=0}^{L} \left(a_i^t\right)^2 \tilde{\mathbf{G}}_l \mathbf{w}^t \left(\mathbf{w}^t\right)^H \tilde{\mathbf{G}}_l^H}{1+z_l^t} \\ & + \frac{c_l^t \sum_{i=0,i\neq l}^{L} \left(a_i^t\right)^2 \tilde{\mathbf{G}}_l \mathbf{w}^t \left(\mathbf{w}^t\right)^H \tilde{\mathbf{G}}_l^H}{1+c_l^t}, \forall l, \\ \boldsymbol{\phi}_l = & \frac{\tilde{\mathbf{H}}_l \mathbf{w}^t \left(\mathbf{w}^t\right)^H \tilde{\mathbf{H}}_l^H \hat{\boldsymbol{\theta}}^t \left(a_l^t\right)^2}{y_l^t} \\ & - \sum_{i=0,i\neq l}^{L} \tilde{\mathbf{G}}_l \mathbf{w}^t \left(\mathbf{w}^t\right)^H \tilde{\mathbf{G}}_l^H \hat{\boldsymbol{\theta}}^t \left(a_i^t\right)^2, \forall l.\end{aligned} \tag{37}$$

When $\hat{\boldsymbol{\theta}}$ is discrete-valued, we introduce the auxiliary variable $\mathbf{u} = \left[u_1, \ldots, u_N, 1\right]^T \in \mathbb{C}^{(N+1)\times 1}$, where $u_n = e^{j\varphi_n}$ satisfies $\mathbf{u} = \hat{\boldsymbol{\theta}}$. Then, following a similar approach as in the previous subsection, we obtain $u_n^\star = e^{j\angle\bar{\varphi}_n}$, where $\bar{\varphi}_n = \arg\min_{\varphi_n \in \mathcal{S}_\varphi} \left|\varphi_n - \angle\left(\theta_n + \rho\lambda_n\right)\right|$.

In addition, when $\hat{\boldsymbol{\theta}}$ is continuous-valued, we apply the element-wise Lagrange dual method to optimize $\hat{\boldsymbol{\theta}}$. Since $|\theta_n| = 1$, by denoting $\Omega_{i,j}$ and ϕ_n as the (i,j)-th element of $\boldsymbol{\Omega}$, and the n-th entry of $\boldsymbol{\phi}$, respectively, we obtain the optimal θ_n as $\theta_n^\star = \tilde{\phi}_n \big/ \left|\tilde{\phi}_n\right|$.

E. Algorithm

We have transformed (7) into a solvable problem and the AO scheme is summarized in Algorithm 4, where $R_s\left(\left\{a_l^t\right\}_{l=0}^{L}, \mathbf{w}^t, \hat{\boldsymbol{\theta}}^t\right)$ represents the obtained value of (7a) in the t-th iteration. According to Theorems 1 and 2 in [35], R_s increases monotonously during the iteration, i.e., $R_s\left(\left\{a_l^{t-1}\right\}_{l=0}^{L}, \mathbf{w}^{t-1}, \hat{\boldsymbol{\theta}}^{t-1}\right) \leq R_s\left(\left\{a_l^t\right\}_{l=0}^{L}, \mathbf{w}^t, \hat{\boldsymbol{\theta}}^t\right)$, which is guaranteed to converge.

Algorithm 4 The algorithm for the proposed AO scheme.

Set $t=0$ and initialize $\left\{\{a_l^0\}_{l=0}^L, \mathbf{w}^0, \hat{\boldsymbol{\theta}}^0\right\}$;
repeat
  Solve (17) to obtain $\{a_l\}_{l=0}^L$ with fixed $\left\{\{a_l^t\}_{l=0}^L, \mathbf{w}^t, \hat{\boldsymbol{\theta}}^t\right\}$;
  Solve (22) to obtain $\mathbf{w}$ with fixed $\left\{\{a_l^t\}_{l=0}^L, \mathbf{w}^t, \hat{\boldsymbol{\theta}}^t\right\}$;
  Solve (36) to obtain $\hat{\boldsymbol{\theta}}$ with fixed $\left\{\{a_l^t\}_{l=0}^L, \mathbf{w}^t, \hat{\boldsymbol{\theta}}^t\right\}$;
  $\left\{\{a_l^{t+1}\}_{l=0}^L, \mathbf{w}^{t+1}, \hat{\boldsymbol{\theta}}^{t+1}\right\} \leftarrow \left\{\{a_l\}_{l=0}^L, \mathbf{w}, \hat{\boldsymbol{\theta}}\right\}$;
  $t \leftarrow t+1$;
until $R_s\left(\{a_l^t\}_{l=0}^L, \mathbf{w}^t, \hat{\boldsymbol{\theta}}^t\right) - R_s\left(\{a_l^{t-1}\}_{l=0}^L, \mathbf{w}^{t-1}, \hat{\boldsymbol{\theta}}^{t-1}\right) \le \varepsilon$ or exceeds the maximum number of iteration;
Output $\left\{\{a_l^\star\}_{l=0}^L, \mathbf{w}^\star, \hat{\boldsymbol{\theta}}^\star\right\}$.

IV. Extension to the SEE design

Compared to the traditional setting with multiple antennas and multiple RF chains, RIS is more energy-efficient. On the other hand, SEE is an effective metric to measure the tradeoff between safety and energy consumption [41]. Thus, in this section, we investigate the SEE design. The total power consumption comes from the transmit power of signals and static circuit power at the feed antenna, refracting RIS, reflective RIS and controllers. Specifically, the total power consumption is modeled as

$$P_{tot} = \frac{P_d}{\xi} + MP(Q_\alpha) + MP(Q_\beta) + NP(Q_\theta), \tag{38}$$

where $P_d = \sum_{l=0}^L a_l^2$ represents the dynamic power to transmit the signal and AN, $0 \le \xi \le 1$ is the power amplifier efficiency factor for the transmitter. Q_α, Q_β, and Q_θ represent the per-element hardware dissipated powers at the RIS with a Q-bit quantization.[1] For the given M, N, Q_α, Q_β, and Q_θ, the term $C = P_c + MP(Q_\alpha) + MP(Q_\beta) + NP(Q_\theta)$ is a constant, and is used to simplify the notation.

The SEE is commonly defined as the ratio of the secrecy rate to the total power consumption [40]. In the considered system, the secrecy rate is actually the weighted sum secrecy rate among all IoTDs. Thus, the formulated optimization problem can be written as

$$\begin{aligned} \max_{\{a_l\}_{l=0}^L, \mathbf{w}, \boldsymbol{\theta}} \quad & \frac{R_s}{\sum_{l=0}^L a_l^2 + C} \\ \text{s.t.} \quad & \text{(7b)} - \text{(7d)}. \end{aligned} \tag{39}$$

Using the Dinkelbach's method and introducing a slack variable η, problem (39) which has a fractional form can be converted to the following linear one

$$\begin{aligned} \max_{\{a_l\}_{l=0}^L, \mathbf{w}, \boldsymbol{\theta}} \quad & R_s - \eta\left(\sum_{l=0}^L a_l^2 + C\right) \\ \text{s.t.} \quad & \text{(7b)}. \end{aligned} \tag{40}$$

The update of η in the t-th iteration is given by [23]

$$\eta^t = \frac{R_s\left(\{a_l^t\}_{l=0}^L, \mathbf{w}^t, \hat{\boldsymbol{\theta}}^t\right)}{\sum_{l=0}^L (a_l^t)^2 + C}. \tag{41}$$

On the other hand, for a given η, (40) can be solved utilizing a quadratic form expression to approximate the non-concave R_s. The main difference is that (40) has the extra term $\eta\left(\sum_{l=0}^L a_l^2 + C\right)$ in the objective. To be specific, around the given point $\left\{\{a_l^t\}_{l=0}^L, \mathbf{w}^t, \hat{\boldsymbol{\theta}}^t, \eta^t\right\}$, we have the following problem with respect to $\{a_l\}_{l=0}^L$ as

$$\begin{aligned} \min_{\{a_l\}_{l=0}^L} \quad & \eta^t \sum_{l=0}^L a_l^2 + \sum_{l=0}^L \left(a_l^2 T_l - 2a_l t_l\right) \\ \text{s.t.} \quad & \text{(7b)}, \end{aligned} \tag{42}$$

which can be solved using Algorithm 1 with $a_l(\lambda) = -t_l/(\lambda + \eta^t + T), \forall l$.

Besides, when given $\left\{\{a_l^t\}_{l=0}^L, \eta^t\right\}$, $\eta\left(\sum_{l=0}^L a_l^2 + C\right)$ is irrelevant with $\mathbf{w}$ and $\hat{\boldsymbol{\theta}}$, the PDD method can be adopted to solve the SEE problem. The solution to the SEE optimization in (39) is summarized as Algorithm 5.

Algorithm 5 The SEE optimization algorithm.

Set $t=0$ and initialize $\left\{\{a_l^0\}_{l=0}^L, \mathbf{w}^0, \hat{\boldsymbol{\theta}}^0, \eta^0\right\}$;
repeat
  Obtain $\left\{\{a_l^t\}_{l=0}^L, \mathbf{w}^t, \hat{\boldsymbol{\theta}}^t\right\}$ by Algorithm 4;
  Update η^t via (41);
  $t \leftarrow t+1$;
until $\left|\eta^t - \eta^{t-1}\right| \le \varepsilon$ or exceeds the maximum number of iteration;
Output $\left\{\{a_l^\star\}_{l=0}^L, \mathbf{w}^\star, \hat{\boldsymbol{\theta}}^\star, \eta^\star\right\}$.

V. Complexity Analysis

In this section, we analyze the computational complexity of the proposed scheme. First, we note that the complexity of optimizing $\{a_l\}_{l=0}^L$ is much lower than that of optimizing $\mathbf{w}$ and $\boldsymbol{\theta}$. Thus, we mainly focus on the optimization of $\mathbf{w}$ and $\boldsymbol{\theta}$. According to [21], the complexity of solving (22) with the PDD method is $\mathcal{O}\left(T_{\mathrm{O}} T_{\mathrm{I}} M^2\right)$, where T_{O} and T_{I} represent the iteration numbers of the outer layer and inner layer, respectively. In contrast, the complexity of solving (22) with the element-wise Lagrange dual method equals $\mathcal{O}\left(T_{\mathrm{E}} M^2\right)$, where T_{E} indicates the number of iterations [35]. Thus, the total computational complexity of Algorithm 4 for the discrete and continuous coefficient case can be, respectively, given as

$$\begin{aligned} \mathcal{C}_{\mathrm{d}} &= \mathcal{O}\left(T_{\mathrm{AO}} T_{\mathrm{O}} T_{\mathrm{I}} \max\left\{M^2, N^2\right\}\right), \\ \mathcal{C}_{\mathrm{c}} &= \mathcal{O}\left(T_{\mathrm{AO}} T_E \max\left\{M^2, N^2\right\}\right), \end{aligned} \tag{43}$$

where T_{AO} stands for the number of iterations of the AO procedure [7].

Moreover, since Algorithm 5 includes one dimensional search of η, its complexity can be estimated as

$$\begin{aligned} \mathcal{C}_{\mathrm{d}} &= \mathcal{O}\left(T_\eta T_{\mathrm{AO}} T_{\mathrm{O}} T_{\mathrm{I}} \max\left\{M^2, N^2\right\}\right), \\ \mathcal{C}_{\mathrm{c}} &= \mathcal{O}\left(T_\eta T_{\mathrm{AO}} T_E \max\left\{M^2, N^2\right\}\right), \end{aligned} \tag{44}$$

for the discrete and continuous coefficient case, respectively, where T_η stands for the search time of η in the outer layer.

[1] According to [4], the power consumption of a single RIS element for 3-bit, 4-bit, 5-bit and 6-bit resolution quantization are given by 1.5 mW, 4.5 mW, 6.0 mW and 7.8 mW, respectively.

VI. Simulation Results

The simulation scenario is illustrated in Fig. 2, there is one transmitter, one reflective RIS, $L = 4$ IoTDs and $L = 4$ Eves, where the transmitter and the RIS are located at $(10\text{m}, 0\text{m}, 10\text{m})$ and $(0\text{m}, 50\text{m}, 10\text{m})$, respectively, while all IoTDs are randomly deployed in a square with side length 10m and centered at $(10\text{m}, 50\text{m}, 1.5\text{m})$. In addition, each Eve is randomly located in a circle with radius 2m and centered around the nearest IoTD.

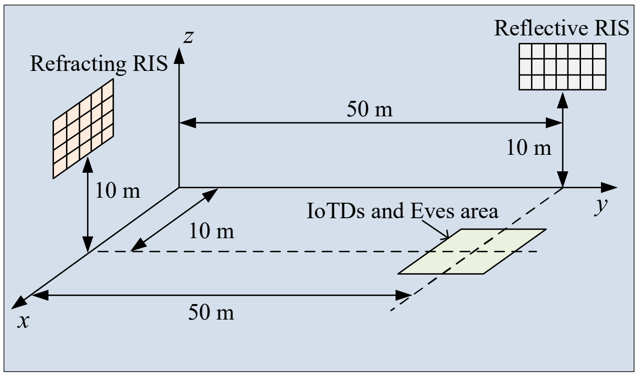

Fig. 2. Simulation scenario.

The following settings are adopted unless otherwise specified: $Q_\alpha/Q_\beta/Q_\theta = 3$, $M = 20$, $N = 60$, $P_s = 0$ dBm, $\sigma_{b,l}^2 = \sigma_{e,l}^2 = -80$ dBm, $\varrho_l = 1/\rho, \forall l$, and $\xi = 0.9$. The path loss is modelled as $\text{PL} = \text{PL}_0 - 10\alpha\log_{10}\left(\frac{d}{d_0}\right)$, where d is the link distance, and α represents the path loss exponent. Here, we set $\text{PL}_0 = -30$ dB and $d_0 = 1\text{m}$. Similar to [35], the path loss exponent of the transmitter to IoTDs/Eves channels is fixed as $\alpha_\text{T} = 4$, and the path loss exponents of the reflective RIS-related channels is set as $\alpha_\text{R} = 2.2$ [38]. Here, we adopt the Rician fading model, and $\mathbf{F}$ is modeled as $\mathbf{F} = \sqrt{\frac{\kappa}{\kappa+1}}\mathbf{F}^{\text{LoS}} + \sqrt{\frac{1}{\kappa+1}}\mathbf{F}^{\text{NLoS}}$, where κ indicates the Rician factor, $\mathbf{F}^{\text{LoS}}$ equals the line-of-sight (LoS) component, and $\mathbf{F}^{\text{NLoS}}$ stands for the non-LoS (NLoS) component which follows a Rayleigh distribution. Here, similar to [35], we set $\beta = 5$ for all the channels. In addition, $\mathbf{F}^{\text{LoS}}$ is given by $\mathbf{F}^{\text{LoS}} = \mathbf{a}_\text{r}\mathbf{a}_\text{t}^H$, where the array response vectors $\mathbf{a}_\text{r}$ and $\mathbf{a}_\text{t}$ are determined by the element array structures at the transmitter and receiver, respectively. Since the RIS is commonly shaped as a uniform planar array, the transmit array response is computed as

$$\begin{aligned}\mathbf{a}_\text{t} = \frac{1}{\sqrt{M}}\Big[&1, \ldots, e^{j2\pi\kappa\left(m\sin\left(\delta_q^\text{t}\right)\sin\left(\psi_q^\text{t}\right)+n\cos\left(\psi_q^\text{t}\right)\right)}, \\ &\ldots, e^{j2\pi\epsilon\left((H-1)\sin\left(\delta_q^\text{t}\right)\sin\left(\psi_q^\text{t}\right)+(V-1)\cos\left(\psi_q^\text{t}\right)\right)}\Big]^T,\end{aligned} \tag{45}$$

where ϵ is the normalized interval between adjacent elements, δ_q^r and δ_q^t denote the azimuth angle and elevation angle of arrivals, and $0 \le m < H$ and $0 \le n < V$ denote the horizontal and vertical RIS element indices, respectively. Thus, the total number of elements is $M = HV$. The receive array response can be defined similarly. Here, we assume that the horizontal orientations of the two RISs are parallel to the x and y axes, respectively, while the vertical orientations of the two RISs are parallel to the z axis. In addition, the scaling factor for the PDD algorithm is set as $\tau = 0.85$ [22].

A. Convergence Property

We assess the convergence of the proposed algorithms, where the entire AO algorithm is named as the outer algorithm, while the PDD or the element-wise Lagrange dual algorithm is called as the inner algorithm.

1) Convergence of the Inner Algorithm: First, for the discrete coefficient case, Fig. 3 shows the weighted sum secrecy rate R_s versus the number of iterations during the PDD process with various transmitter or RIS element numbers. From Fig. 3, we can observe that R_s increases with the number of iterations, and converges within 100 iterations for the different M and N combinations considered. In addition, we can see that there is fluctuation in the obtained curves. This phenomenon is caused by the updating of the dual variable and penalty factor. Specifically, when the initial penalty factor ρ is relatively large, the obtained solution does not satisfy the constraint $\mathbf{w} = \mathbf{r}$ in problem (24), thus resulting in the oscillatory behavior. While as ρ decreases with increasing iterations, the constraint violation is forced to approach the predefined accuracy ε. Thus, the secrecy rate performance fluctuation with the iteration number becomes smaller. Similar results can also be observed in related works such as [20]–[22].

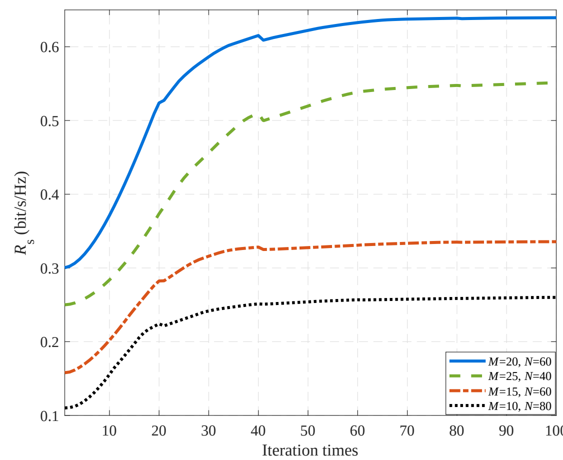

Fig. 3. Convergence of the PDD algorithm.

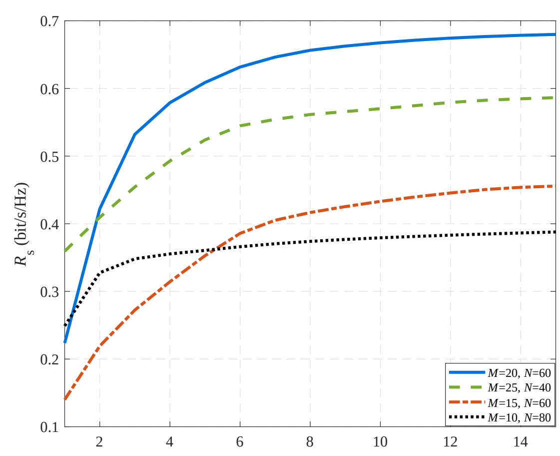

Fig. 4. Convergence of the dual algorithm.

Then, we examine the convergence of the element-wise

Lagrange dual method in the continuous coefficient case. From Fig. 4, we can see that for different numbers of transmitter or reflective RIS elements, the proposed element-wise Lagrange dual method converges within 15 iterations. In addition, by comparing the curves in Figs. 3 and 4, we confirm that the discrete coefficient case suffers from a certain performance loss due to the effect of quantization errors caused by the limited number of quantization bits.

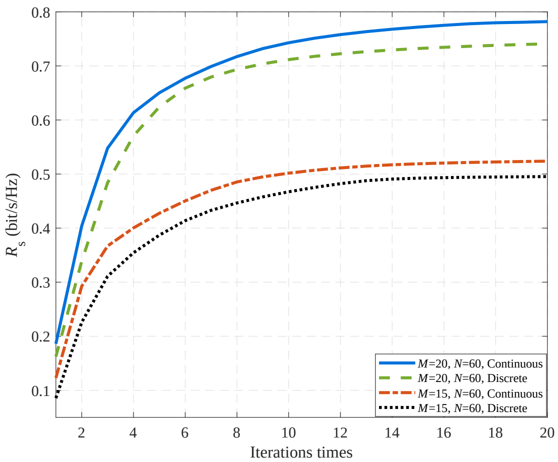

Fig. 5. Convergence of the AO algorithm.

2) Convergence of the AO Method: Now, we examine the convergence of the AO algorithm for both the discrete and continuous coefficients cases. Fig. 5 shows R_s versus the number of iterations for different M and N, where we can see that a larger M or N results in a higher secrecy rate, at the cost of more iterations. However, for the different M and N combinations considered, the AO algorithm always converges within 20 iterations, which confirms the efficiency of the proposed algorithm.

B. Performance Evaluation

We study the performance of the proposed design and compare it with the following benchmarks: 1) traditional transmitter, which performs BF and emits AN via multiple RF chains and antennas [35]; 2) equal power allocation method, where the transmitter allocates the same power to each confidential signal and the AN; 3) fixing the amplitude of the refracting RIS to be 1, e.g., setting $\alpha_m = 1, \forall m \in \mathcal{M}$; 4) random reflective RIS, which chooses $\boldsymbol{\theta}$ randomly; 5) without reflective RIS; 6) the alternating direction method of multiplier (ADMM) algorithm. These methods are labelled as "Continuous", "Discrete", "Traditional transmitter", "Equal power allocation", "Fixed Amplitude", "Random RIS method", "No-RIS method", and "ADMM algorithm", respectively.[2]

Fig. 6 depicts the weighted sum secrecy rate versus P_s, where we can see that R_s increases with P_s. The traditional transmitter achieves the best secrecy performance mainly due to the use of multiple RF chains and antennas to generate different BF vectors to align the information to different users [35]. The RIS-based transmitter structure exhibits lower

[2]Here, the discrete coefficient means that $\{\alpha_m, \beta_m, \varphi_n\}$ are all discrete, while the continuous coefficient means that $\{\alpha_m, \beta_m, \varphi_n\}$ are all continuous.

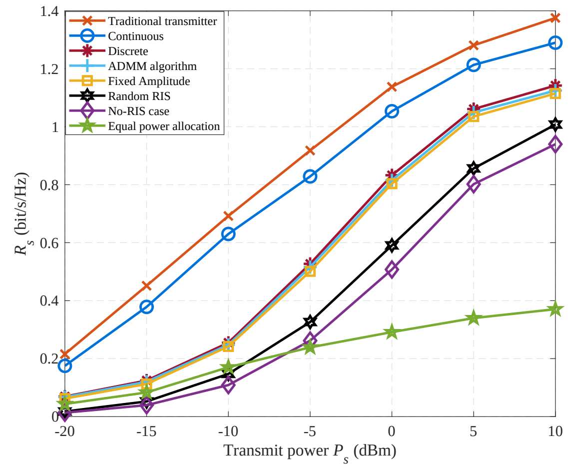

Fig. 6. R_s versus P_s.

performance compared with the traditional transmitter, but the performance gap is not so evident. Also, the random RIS scheme outperforms the no-RIS-assisted scheme. In fact, in the low P_s region, no matter which kind of power allocation strategy is used, the receive noise is the dominant factor for the performance, while in the high P_s region, the interference between users becomes the main performance limiting factor. Thus, equal power allocation scheme is highly suboptimal in allocating the signal power among different users, thus leading to a performance loss, especially as P_s increases. Besides, we can observe that the proposed PDD method outperforms the ADMM algorithm due to the expanded search space. Moreover, the fixed modulus design suffers from a certain performance loss when compared with the proposed design, because the fixed amplitude design can not adapt to the rapidly changing channels. When the channel quality of Eves are better than that of IoTDs, it is better to use partial transmit power to transmit the confidential signal.

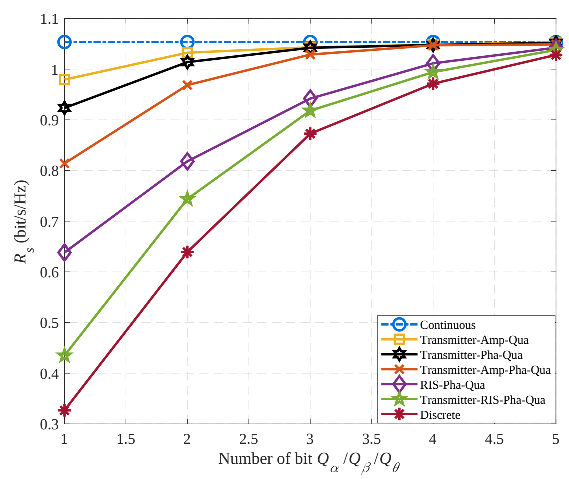

Fig. 7. R_s versus $Q_\alpha/Q_\beta/Q_\theta$.

To closely examine the effect of quantization, Fig. 7 shows R_s versus $Q_\alpha/Q_\beta/Q_\theta$ with different quantization schemes, where the meaning of "Continuous" and "Discrete" are the same as in Fig. 6, e.g., no quantization or full quantization of $\mathbf{w}$ and $\boldsymbol{\theta}$. While "RIS-Pha-Qua", "Transmitter-Pha-

Qua", "Transmitter-RIS-Pha-Qua", "Transmitter-Amp-Qua", and "Transmitter-Amp-Pha-Qua" denote the quantization of $\boldsymbol{\theta}$, the quantization of the phase of $\mathbf{w}$, the quantization of $\boldsymbol{\theta}$ and the phase of $\mathbf{w}$, the quantization of the amplitude of $\mathbf{w}$, and the quantization of both the amplitude and phase of $\mathbf{w}$, respectively. From Fig. 7, we can see that for different quantization methods, R_s increases with the number of bits and converges to its value in the continuous coefficient case. It can also be observed from Fig. 7 that the effect of coefficient phase quantization is more dominating than the coefficient amplitude quantization. This is mainly due to the fact that the corresponding amplitude of w_m in the continuous coefficient case is very close to 1 in most simulation realizations, thus when quantizing it, the performance loss is marginal.

Then, Fig. 8 depicts the obtained weighted sum secrecy rate and sum secrecy rate of the proposed design versus the number of the IoTD/Eves L. From this figure, we can see that the proposed scheme can achieve satisfactory secrecy performance with different L, where the sum secrecy rate increases with L and the weighted sum secrecy rate decreases with L. This is mainly due to the fact that when the number of IoTD increases, the inter-user interference becomes more serious, thus the sum secrecy rate grows more slowly. On the other hand, since we set the weight for each IoTD as $1/L$, e.g., the weight decreases with L, the weighted sum secrecy rate decreases with L.

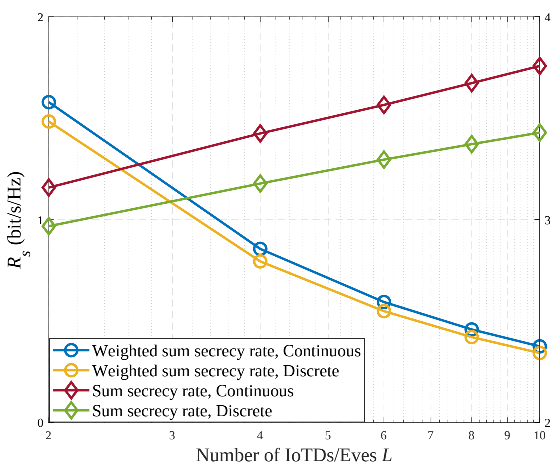

Fig. 8. Sum secrecy rate or R_s versus L.

Next, we compare the SEE of several schemes versus P_s in Fig. 9. To be specific, the curve labelled "Rate-oriented" denotes the design which aims to maximize R_s without considering the power consumption, while the other curves are all SEE-oriented. From this figure, we can observe that the RIS-based transmitter outperforms the traditional transmitter due to the reduced number of RF chains and antennas. Besides, for all SEE-oriented schemes, the SEE tends to increase with P_s, then remains saturated. This behavior is due to the fact that there exists a unique optimal P_s for SEE design and the SEE will saturate when P_s exceeds the optimal value. However, the SEE for the rate-oriented design decreases in the relatively high P_s region, since all achievable P_s is exploited to maximize R_s, thus a large P_s leads to a drop in SEE. In addition, by comparing the curves of "Continuous" and "Discrete", we find that having more quantization bits leads to the degradation of SEE, since the improvement of R_s is very limited when compared with the extra power consumption introduced by more quantization bits.[3]

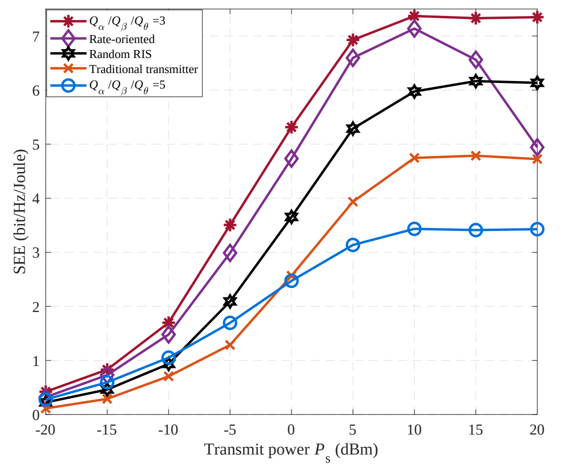

Fig. 9. SEE versus P_s.

Lastly, we compare the SEE versus the number M and N in Figs. 10 and 11, where we find that SEE does not increase monotonically with M or N, and there exists a SEE-optimal value for M or N. Thus, it is important to strike a balance between the SE obtained by utilizing larger RIS and the corresponding cost of the power consumption. In addition, similar to the previous results, the PDD method achieves better SEE performance than the ADMM algorithm and the fixed amplitude design, since when given the same parameters, the PDD method can achieve better secrecy rate performance than the two benchmarks.

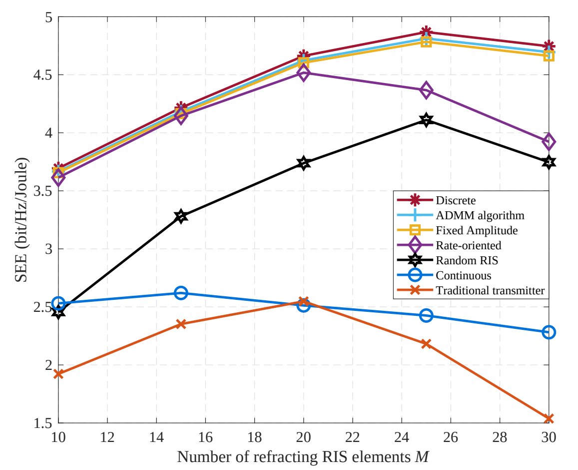

Fig. 10. SEE versus M.

VII. CONCLUSION

In this paper, we investigated the application of an active refracting RIS-enabled transmitter for a secure IoT network. To

[3]The curve labelled "Continuous" is actually achieved by adapting the 5-bit quantization for $\mathbf{w}$ and $\boldsymbol{\theta}$, which approaches the weighted sum secrecy rate performance with the continuous coefficients case, as shown in Fig. 7, while all the other curves are obtained by using 3-bit quantization for $\mathbf{w}$ and $\boldsymbol{\theta}$.

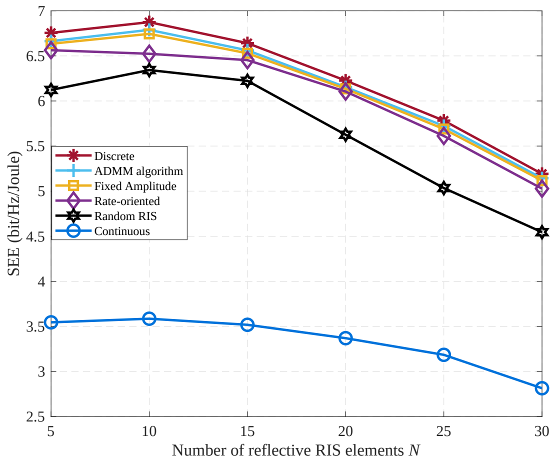

Fig. 11. SEE versus N.

enhance secure communication of the considered network, we developed an AO algorithm to optimize the sum secrecy rate by jointly designing the power allocation, transmit BF, and the phase shifts of the RIS, where the original nonconvex problem was converted into three subproblems and efficiently solved by the proposed AO scheme iteratively. Then, we extended the proposed scheme to the SEE maximization problem by using the Dinkelbach's method. Simulation results verified the advantages of the proposed design for achieving higher energy efficiency with fast convergence compared to other benchmark schemes. Besides, the above figures can help the designer in selecting the optimal number of RIS elements in terms of SEE for practical application.

REFERENCES

[1] Z. Lin, M. Lin, *et al.*, "Supporting IoT with rate-splitting multiple access in satellite and aerial integrated networks," *IEEE Inter. Things J.*, vol. 8, no. 14, pp. 11123–11134, Jul. 2021.

[2] Q. Wu, S. Zhang, *et al.*, "Intelligent reflecting surface aided wireless communications: A tutorial," *IEEE Trans. Commun.*, vol. 69, no. 5, pp. 3313–3351, May. 2021.

[3] Y. Liu, X. Liu, *et al.*, "Reconfigurable intelligent surfaces: Principles and opportunities," *IEEE Commun. Surv. Tut.*, vol. 23, no. 3, pp. 1546–1577, 3rd Quart. 2021.

[4] C. Huang, A. Zappone, *et al.*, "Reconfigurable intelligent surfaces for energy efficiency in wireless communication," *IEEE Trans. Wireless Commun.*, vol. 18, no. 8, pp. 4157–4170, Aug. 2019.

[5] J. Woo, C. Song, and I. Lee, "Sum rate and fairness optimization for intelligent reflecting surface aided multiuser systems," *IEEE Trans. Veh. Tech.*, vol. 70, no. 12, pp. 13436–13440, Dec. 2021.

[6] G. Zhou, C. Pan, *et al.*, "Intelligent reflecting surface aided multigroup multicast MISO communication systems," *IEEE Trans. Signal Process.*, vol. 68, pp. 3236–3251, Apr. 2020.

[7] C. Pan, H. Ren, *et al.*, "Multicell MIMO communications relying on intelligent reflecting surface," *IEEE Trans. Wireless Commun.*, vol. 19, no. 8, pp. 5218–5233, Aug. 2020.

[8] Z. Yang, M. Chen, et al, "Energy-efficient wireless communications with distributed reconfigurable intelligent surfaces," *IEEE Trans. Wireless Commun.*, vol. 21, no. 11, pp. 665–679, Jan. 2022.

[9] Z. Chu, Z. Zhu, *et al.*, "Intelligent reflecting surface assisted wireless powered sensor networks for internet of things," *IEEE Trans. Commun.*, vol. 69, no. 7, pp. 4877–4889, Jul. 2021.

[10] X. Xie, C. He, *et al.*, "A joint optimization framework for IRS-assisted energy self-sustainable IoT networks," *IEEE Inter. Things J.*, vol. 9, no. 15, pp. 13767–13779, Aug. 2022.

[11] Z. Zhu, Z. Li, *et al.*, "Resource allocation for intelligent reflecting surface assisted wireless powered IoT systems with power splitting," *IEEE Trans. Wireless Commun.*, vol. 21, no. 5, pp. 2987–2998, May 2022.

[12] Z. Li, W. Chen, *et al.*, "Joint beamforming design and power splitting optimization in IRS-assisted SWIPT NOMA networks," *IEEE Trans. Wireless Commun.*, vol. 21, no. 3, pp. 2019–2033, Mar. 2022.

[13] Y. Sun, K. An, *et al.*, "Energy-efficient hybrid beamforming for multi-layer RIS-assisted secure integrated terrestrial-aerial networks," *IEEE Trans. Commun.*, vol. 70, no. 6, pp. 4189–4210, Jun. 2022.

[14] Z. Lin, H. Niu, *et al.*, "Refracting RIS aided hybrid satellite-terrestrial relay networks: Joint beamforming design and optimization," *IEEE Trans. Aerosp. Electron. Syst.*, vol. 58, no. 4, pp. 3717–3724, Aug. 2022.

[15] Y. Sun, K. An, *et al.*, "Outage constrained robust beamforming optimization for multiuser IRS-assisted anti-jamming communications with incomplete information," *IEEE Inter. Things J.*, vol. 9, no. 15, pp. 13298–13314, Aug. 2022.

[16] Y. Sun *et al.*, "Robust design for RIS-assisted anti-jamming communications with imperfect angular information: A game-theoretic perspective," *IEEE Trans. Veh. Tech.*, vol. 71, no. 7, pp. 7967–7972, Jul. 2022.

[17] Y. Sun, K. An, *et al.*, "Intelligent reflecting surface enhanced secure transmission against both jamming and eavesdropping attacks," *IEEE Trans. Veh. Tech.*, vol. 70, no. 10, pp. 11017–11022, Oct. 2021.

[18] Y. Sun, K. An, *et al.*, "RIS-assisted robust hybrid beamforming against simultaneous jamming and eavesdropping attacks," *IEEE Trans. Wireless Commun.*, early access, May 2022, doi: 10.1109/TWC.2022.3174629.

[19] Y. Wu, F. Zhou, *et al.*, "Multi-objective optimization for spectrum and energy efficiency tradeoff in IRS-assisted CRNs with NOMA," *IEEE Trans. Wireless Commun.*, vol. 21, no. 8, pp. 6627–6642, Aug. 2022.

[20] M.-M. Zhao, A. Liu, and R. Zhang, "Outage-constrained robust beamforming for intelligent reflecting surface aided wireless communication," *IEEE Trans. Signal Process.*, vol. 69, pp. 1301–1316, Feb. 2021.

[21] M.-M. Zhao, Q. Wu, *et al.*, "Intelligent reflecting surface enhanced wireless network: Two-timescale beamforming optimization," *IEEE Trans. Wireless Commun.*, vol. 20, no. 1, pp. 2–17, Jan. 2021.

[22] Y. Liu, J. Zhao, M. Li, and Q. Wu, "Intelligent reflecting surface aided MISO uplink communication network: Feasibility and power minimization for perfect and imperfect CSI," *IEEE Trans. Commun.*, vol. 69, no. 3, pp. 1975–1989, Mar. 2021.

[23] L. You, J. Xiong, *et al.*, "Reconfigurable intelligent surfaces-assisted multiuser MIMO uplink transmission with partial CSI," *IEEE Trans. Wireless Commun.*, vol. 20, no. 9, pp. 5613–5627, Sep. 2021.

[24] L. You, J. Xiong, *et al.*, "Energy efficiency and spectral efficiency tradeoff in RIS-aided multiuser MIMO uplink transmission," *IEEE Trans. Signal Process.*, vol. 69, pp. 1407–1421, 2021.

[25] S. Guo, S. Lv, *et al.*, "Reflecting modulation," *IEEE J. Sel. Areas Commun.*, vol. 38, no. 11, pp. 2548–2561, Nov. 2020.

[26] E. Basar, "Reconfigurable intelligent surface-based index modulation: A new beyond MIMO paradigm for 6G," *IEEE Trans. Commun.*, vol. 68, no. 5, pp. 3187–3196, May 2020.

[27] J. Zhao, X. Yang, *et al.*, "Programmable time-domain digital-coding metasurface for non-linear harmonic manipulation and new wireless communication systems," *National Science Review*, vol. 6, no. 2, pp. 231–238, Mar. 2019.

[28] J. Dai, W. Tang, *et al.*, "Wireless communications through a simplified architecture based on time-domain digital coding metasurface," *Advanced Materials Technologies*, vol. 4, no. 7, pp. 1–8, Jul. 2019.

[29] W. Tang, J. Dai, *et al.*, "MIMO transmission through reconfigurable intelligent surface: System design, analysis, and implementation," *IEEE J. Sel. Areas Commun.*, vol. 38, no. 11, pp. 2683–2699, Nov. 2020.

[30] L. Zhang, M. Chen, *et al.*, "A wireless communication scheme based on space and frequency division multiplexing using digital metasurfaces," *Nature Electronics*, vol. 4, pp. 218–227, Mar. 2021.

[31] M. Chen, W. Tang, *et al.*, "Accurate and broadband manipulations of harmonic amplitudes and phases to reach 256QAM millimeter-wave wireless communications by time-domain digital coding metasurface," *National Science Review*, Jul. 2021.

[32] Z. Li and W. Chen, "Transmissive reconfigurable meta-surface empowered 6G ultra massive MIMO," 2021, *arXiv: 2109.05462v1*, [Online]. Available:https://arxiv.org/abs/2109.05462.

[33] Z. Li, W. Chen, and H. Cao, "Beamforming design and power allocation for transmissive RMS-based transmitter architectures," *IEEE Wireless Commun. Lett.*, vol. 11, no. 1, pp. 53–57, Jan. 2022.

[34] Z. Li, W. Chen, *et al.*, "Uplink transceiver design and optimization for transmissive RMS multi-antenna systems," 2021, *arXiv: 2112.08880v1*, [Online]. Available:https://arxiv.org/abs/2112.08880.

[35] H. Niu, Z. Chu, *et al.*, "Weighted sum secrecy rate maximization using intelligent reflecting surface," *IEEE Trans. Commun.*, vol. 69, no. 9, pp. 6170–6184, Sep. 2021.

[36] H. Wang, J. Bai, and L. Dong, "Intelligent reflecting surfaces assisted secure transmission without eavesdropper's CSI," *IEEE Signal Process. Lett.*, vol. 27, pp. 1300–1304, Jul. 2020.
[37] H. Niu, Z. Chu, *et al.*, "Robust design for intelligent reflecting surface assisted secrecy SWIPT network," *IEEE Trans. Wireless Commun.*, vol. 21, no. 6, pp. 4133–4149, Jun. 2022.
[38] S. Hong, C. Pan, *et al.*, "Robust transmission design for intelligent reflecting surface aided secure communication systems with imperfect cascaded CSI," *IEEE Trans. Wireless Commun.*, vol. 20, no. 4, pp. 2487–2501, Apr. 2021.
[39] Z. Chu, W. Hao, *et al.*, "Secrecy rate optimization for intelligent reflecting surface assisted MIMO system," *IEEE Trans. Inf. Forensics Security*, vol. 16, pp. 1655–1669, Nov. 2020.
[40] Q. Wang, F. Zhou, R. Q. Hu, and Y. Qian, "Energy efficient robust beamforming and cooperative jamming design for IRS-assisted MISO networks," *IEEE Trans. Wireless Commun.*, vol. 20, no. 4, pp. 2592–2607, Apr. 2021.
[41] Z. Lin, M. Lin, *et al.*, "Secure and energy efficient transmission for RSMA-based cognitive satellite-terrestrial networks," *IEEE Wireless Commun. Lett.*, vol. 10, no. 2, pp. 251–255, Feb. 2021.
[42] S. Gong, Z. Yang, *et al.*, "Beamforming optimization for intelligent reflecting surface-aided SWIPT IoT networks relying on discrete phase shifts," *IEEE Inter. Things J.*, vol. 8, no. 10, pp. 8585–8602, May, 2021.
[43] M.-M. Zhao, Q. Wu, *et al.*, "Exploiting amplitude control in intelligent reflecting surface aided wireless communication with imperfect CSI," *IEEE Trans. Commun.*, vol. 69, no. 6, pp. 4216–4231, Jun. 2021.
[44] A. A. Nasir, H. D. Tuan, *et al.*, "Secrecy rate beamforming for multicell networks with information and energy harvesting," *IEEE Trans. Signal Process.*, vol. 65, no. 3, pp. 677–689, Feb. 2017.
[45] Z. Lin, M. Lin, J.-B. Wang, *et al.*, "Joint beamforming and power allocation for satellite-terrestrial integrated networks with non-orthogonal multiple access," *IEEE J. Sel. Topics Signal Process.*, vol. 13, no. 3, pp. 657–670, Jun. 2019.
[46] Z. Lin, K. An, H. Niu, *et al.*, "SLNR-based secure energy efficient beamforming in multibeam satellite systems," *IEEE Trans. Aerosp. Electron. Syst.*, early access, Jul. 2022, doi: 10.1109/TAES.2022.3190238.
[47] Q. Li, C. Li, and J. Lin, "Constant modulus secure beamforming for multicast massive MIMO wiretap channels," *IEEE Trans. Inf. Forensics Security*, vol. 15, pp. 264–275, Jul. 2020.
[48] M. Grant and S. Boyd, CVX: Matlab software for disciplined convex programming, version 2.0 beta, 2012. [online]. Available: http://cvxr.com/cvx.
[49] Q. Shi and M. Hong, "Penalty dual decomposition method for nonsmooth nonconvex optimization-Part I: Algorithms and convergence analysis," *IEEE Trans. Signal Process.*, vol. 68, pp. 4108–4122, Jun. 2020.

Hehao Niu is currently a engineer with the Sixty-third Research Institute, National University of Defense Technology, Nanjing, China. His current research interests include smart radio environments/smart reflecting surface, 5G/6G communication networks, unmanned aerial vehicle communication, machine learning, wireless physical layer security, and anti-jamming communication, etc.

Zhi Lin received the B.E. and M.E. degrees in information and communication engineering from the PLA University of Science and Technology and the Ph.D. degree in electronic science and technology from the Army Engineering University of PLA, Nanjing, China, in 2013, 2016, and 2020, respectively. From March 2019 to June 2020, he was a visiting Ph.D. student with the Department of Electrical and Computer Engineering, McGill University, Montréal, Canada. He is currently an Assistant Professor with the College of Electronic Engineering, National University of Defense Technology, Hefei, China.

Dr. Lin's research interests include the general area of wireless communications and array signal processing, and in particular in the area of Satellite-Terrestrial Integrated Networks (STIN). He was the Symposium Co-Chair of IEEE WCSP'22 and TPC members of IEEE sponsored conferences, including IEEE ICC, Globecom, Infocom, VTC, and so on. He was the recipient of the Outstanding Ph.D. Thesis Award of Chinese Institute of Electronics in 2022 and the Macao Young Scholars Fellowship in 2022.

Zheng Chu (Member, IEEE) received the Ph.D. degree from Newcastle University, Newcastle upon Tyne, United Kingdom, in 2016. He was with the Faculty of Science and Technology, Middlesex University, London, United Kingdom, from 2016 to 2017. He is currently with the Institute for Communication Systems, University of Surrey, Guildford, United Kingdom. His current research interests include smart radio environments/smart reflecting surface, 5G/6G communication networks, Internet of Things (IoT) networks, Artificial Intelligence (AI) driven future networks, wireless security, wireless powered networks.

Zhengyu Zhu (Senior Member, IEEE) received the Ph.D. degree in information engineering from Zhengzhou University, Zhengzhou, China, in 2017. From October 2013 to October 2015, he visited the Communication and Intelligent System Laboratory, Korea University, Seoul, South Korea, to conduct a collaborative research as a Visiting Student. He is currently an associate professor with Zhengzhou University. He served as an Associate Editor for the JOURNAL OF COMMUNICATIONS AND NETWORKS, the WIRELESS COMMUNICATIONS AND MOBILE COMPUTING, and the PHYSICAL COMMUNICATIONS from 2021.His research interests include information theory and signal processing for wireless communications such as B5G/6G, Intelligent reflecting surface, the Internet of Things, machine learning, millimeter wave communication, UAV communication, physical layer security, convex optimization techniques, and energy harvesting communication systems.

Pei Xiao (Senior Member, IEEE) is a professor of Wireless Communications at the Institute for Communication Systems (ICS), home of 5GIC and 6GIC at the University of Surrey. He received the PhD degree from Chalmers University of Technology, Gothenburg, Sweden in 2004. He is currently the technical manager of 5GIC/6GIC, leading the research team in the new physical layer work area, and coordinating/supervising research activities across all the work areas (https://www.surrey.ac.uk/institute-communication-systems/5g-6g-innovation-centre). Prior to this, he worked at Newcastle University and Queen's University Belfast. He also held positions at Nokia Networks in Finland. He has published extensively in the fields of communication theory, RF and antenna design, signal processing for wireless communications, and is an inventor on over 15 recent 5GIC patents addressing bottleneck problems in 5G systems.

Huan X. Nguyen (M'06–SM'15) received the B.Sc. degree from the Hanoi University of Science and Technology, Vietnam, in 2000, and the Ph.D. degree from the University of New South Wales, Australia, in 2007. He is currently a Professor of Digital Communication Engineering at Middlesex University London (U.K.), where he is also the Director of the London Digital Twin Research Centre and Head of the 5G/6G & IoT Research Group. He leads research activities in digital twin modelling, 5G/6G systems, machine-type communication, digital transformation and machine learning within his university with focus on industry 4.0 and critical applications (disasters, intelligent transportation, health). He has been leading major council/industry funded projects, publishing 130+ peer-reviewed research papers, and serving as chairs for international conferences (ICT'21, ICEM2021, ICT'20, ICT'19, IWNPD'17, PIMRC'20, FoNeS-IoT'20, ATC'15). He is a Senior Member of the IEEE and a Senior Fellow of the HEA.

Inkyu Lee (Fellow, IEEE) received the B.S. degree (Hons.) in control and instrumentation engineering from Seoul National University, Seoul, South Korea, in 1990, and the M.S. and Ph.D. degrees in electrical engineering from Stanford University, Stanford, CA, USA, in 1992 and 1995, respectively. From 1995 to 2002, he was a member of the Technical Staff with Bell Laboratories, Lucent Technologies, Murray Hill, NJ, USA, where he studied high-speed wireless system designs. Since 2002, he has been with Korea University, Seoul, where he is currently a Professor with the School of Electrical Engineering. He has also served as the Department Head of the School of Electrical Engineering, Korea University, from 2019 to 2021. In 2009, he was a Visiting Professor with the University of Southern California, Los Angeles, CA, USA. He has authored or coauthored more than 200 journal articles in IEEE publications and holds 30 U.S. patents granted or pending. His research interests include digital communications and signal processing techniques applied for next-generation wireless systems. He was elected as a member of the National Academy of Engineering of Korea in 2015. He was a recipient of the IT Young Engineer Award at the IEEE/IEEK Joint Award in 2006, the Best Paper Award at the IEEE Vehicular Technology Conference in 2009, the Best Research Award from the Korean Institute of Communications and Information Sciences in 2011, the Best Paper Award at the IEEE International Symposium on Intelligent Signal Processing and Communication Systems in 2013, the Best Young Engineer Award from the National Academy of Engineering of Korea in 2013, and the Korea Engineering Award from the National Research Foundation of Korea in 2017. He served as an Associate Editor for the IEEE TRANSACTIONS ON COMMUNICATIONS from 2001 to 2011 and the IEEE TRANSACTIONS ON WIRELESS COMMUNICATIONS from 2007 to 2011. In addition, he was a Chief Guest Editor of the IEEE JOURNAL ON SELECTED AREAS IN COMMUNICATIONS Special Issue on "4G wireless systems" in 2006. He also serves as the Co-Editor-in-Chief for the Journal of Communications and Networks. Currently he is the director of "Augmented Cognition Meta-Communication" ERC research center awarded from the National Research Foundation of Korea. He is also a Distinguished Lecturer of IEEE.

Naofal Al-Dhahir (Fellow, IEEE) is Erik Jonsson Distinguished Professor & ECE Associate Head at UT-Dallas. He earned his PhD degree from Stanford University and was a principal member of technical staff at GE Research Center and AT&T Shannon Laboratory from 1994 to 2003. He is co-inventor of 43 issued patents, co-author of about 500 papers and co-recipient of 5 IEEE best paper awards. He is an IEEE Fellow, AAIA Fellow, received 2019 IEEE SPCC technical recognition award and 2021 Qualcomm faculty award.

He served as Editor-in-Chief of IEEE Transactions on Communications from Jan. 2016 to Dec. 2019. He is a Fellow of the US National Academy of Inventors.